Studying Λ interactions in nuclear matter with the $^{208}Pb(e,e'K^+)^{208}_{\Lambda}Tl$ reaction

Spokespersons

O. Benhar[1], F. Garibaldi[1], P.E.C. Markowitz[2], S.N. Nakamura[3], J.Reinhold[2] , L. Tang[4], G..M. Urciuoli[1]*
** Contact person*

1. *INFN Roma1*
2. *Florida International University*
3. *Graduate School of Science, Tohoku University*
4. *Department of Physics, Hampton University*
   Thomas Jefferson National Accelerator Facility (JLab)

JLab Hypernuclear Collaboration:

A. Lovato
Argonne National Laboratory
D.J. Millener
Brookhaven National Laboratory
K. Aniol
California State University
T. Horn
Catholic University of America
F. Benmokhtar
Duquesne University
P.E.C. Markowitz (spokesperson), J. Reinhold (spokesperson)
Florida International University
P. Gueye, B.Pandey, L. Tang (spokesperson)
Physics Department, Hampton University
G. De Cataldo, R. De Leo, D. Di Bari, L. Lagamba, E. Nappi
INFN/ Bari
V. Bellini, P. Castorina, V. Kuznetsov, F. Mammoliti, C.M.A. Petta, G.E. Poma, L. Re, G. Russo, M. Russo, A. Shahinyan, S. Spinali, C.M. Sutera
INFN/ ,
I. Balossino, L. Barion, G. Ciullo, M. Contalbrigo, A. Drago, P. Lenisa, A. Movsisyan, L.L. Pappalardo, F. Spizzo, I. Vidana
INFN/ Ferarra
V. Lucherini, M. Mirazita, P. Rossi
INFN/ Frascati
M. Battaglieri, G. Bracco, A. Brunengo, A. Celentano, R. De Vita, S. Grazzi, L. Marsicano, V. Mathieu, P. Musico, M. Osipenko, L. Perasso, M. Ripani
INFN/ Genova
R. Perrino
INFN/ Lecce
G. Simi
INFN/ Padova
M. Carpinelli, G. Contino, D. D'Urso, A. Gabrieli, V. Sipala
INFN/ LNS

O. Benhar (spokesperson), E. Cisbani, F. De Persio, A. Del Dotto, F. Garibaldi (spokesperson and contact person)), F. Meddi, C.A. Nicolau, G.M. Urciuoli (spokesperson) *INFN/ Rome*
A. D'Angelo, L. Lanza, A. Rizzo
INFN/ Rome Tor Vergata
A. Filippi, M. Genovese
INFN/ Torino
T. Takahashi, Y. Sato
Institute for Particle and Nuclear Physics, KEK
T. Holmstrom
Longwood University
S. Gandolfi
Theoretical Division, Los Alamos national Laboratory
J. Pochodzalla, P.Achenbach
Institute fur KernPhysik, Johannes Gutenberg University Mainz
A. Ahmidouch, S. Danagoulian,
North Carolina A&T State University
S. Covrig, S.C. Dusa, C. Keppel, S.A. Wood
Thomas Jefferson National Accelerator Facility
D. Lonardoni
National Superconducting Cyclotron Laboratory, Michigan State University and
Theoretical Division, Los Alamos National Laboratory
F.R. Wesselmann
Old Dominion University
E. Hiyama, M. Isaka, Y.Yamamoto
RIKEN
M. Elaasar
Southern University at New Orleans
P. Bydžovský
Nuclear Physics Institute, Řež near Prague
T. Motoba
Laboratory of Physics, Osaka Electro-Communication University
V. M. Rodriguez
Universidad Metropolitana, San Juan, Puerto Rico
G. Aida, M.Fujita, T. Gogami, M. Kaneta, H. Kanda, K. Maeda, S. Nagao,
S.N. Nakamura (spokesperson), H. Takeuchi, S. Tomita, Y.Toyama, Y.Muroi
Graduate School of Science, Tohoku University
Y. Fujii
Tohoku Medical and Pharmaceutical University
F. Pederiva
Physics Department, University of Trento and INFN-TIFPA
C. Samanta
Dept. of Physics & Astronomy, Virginia Military Institute
J. Hoskins
College of William and Mary
A. Margaryan
Yerevan Physics Institute, Yerevan, Armenia
D. Androic, M. Furic
Department of Physics, University of Zagreb
T. Petkovic
Faculty of Electrical Engineering and Computing, Department of Applied Physics, University of Zagreb

V. M. Rodriguez
Universidad Metropolitana, San Juan, Puerto Rico
G. Aida, M.Fujita, M. Kaneta, H. Kanda, K. Maeda, S. Nagao,
S.N. Nakamura (spokesperson), H. Takeuchi, S. Tomita, Y.Toyama, Y.Muroi
Graduate School of Science, Tohoku University
Y. Fujii
Tohoku Medical and Pharmaceutical University
F. Pederiva
Physics Department, University of Trento and INFN-TIFPA
C. Samanta
Dept. of Physics & Astronomy, Virginia Military Institute
Abstract
College of William and Mary
A. Margaryan
Yerevan Physics Institute, Yerevan, Armenia
D. Androic, M. Furic
Department of Physics, University of Zagreb
T. Petkovic
Faculty of Electrical Engineering and Computing, Department of Applied Physics, University of Zagreb

Abstract

An ambitious and challenging experimental program, aimed at obtaining high-resolution hypernuclear spectroscopy via the (e,e'K^+) reaction, was started at Jefferson Lab 15 years ago. The data, taken in both Hall A and Hall C using p-shell and medium-mass nuclear targets, have provided clear spectra with 0.5~0.8-MeV energy resolution. The process, whose feasibility has been established at JLab, is now widely recognized as a powerful tool to study hypernuclear spectroscopy, in addition to the (K^-, π^-) and (π^+, K^+) reactions. Electron- and hadron-induced reactions are in fact complementary to one another, being predominantly driven by spin-flip and non-spin-flip mechanisms, respectively. Furthermore, the (e,e'K^+) reaction allows us for a much better energy resolution and produces mirror hypernuclei with respect to those produced with hadron probes.

The 6 GeV experiments provided the experience needed to confidently set up a new program for the 12 GeV era. It should be noted that the new optimized experimental design not only widens and deepens the physics investigation range and topics, but also dramatically improves on the data quality and production efficiency, maximizing the physics output.

The recent observation of two-solar-mass neutron stars rules out most of the current models of hyperonic matter equation of state, which favour the appearance of hyperons in the neutron star interior but predict maximum masses (M_{max}) incompatible with data. This issue, referred to as "hyperon puzzle", strongly suggests that the present understanding of nuclear interactions involving hyperons is far form being complete.

Owing to the severe difficulties involved in the extraction of the potential describing YN interactions from YN scattering data, the study of hypernuclear spectroscopy appears to be the most effective approach to obtain new information, much needed to unravel the hyperon puzzle.

For this reason the JLab hypernuclear collaboration proposed to PAC43 a coherent series of studies of the (e,e'K^+) reaction, to be performed using targets spanning a wide range of mass. The purpose of this analysis was investigation of the ΛN interactions in a variety of nuclear media. The PAC43 identified the study of the isospin dependence as the highest priority, and conditionally approved the $^{40}_{\Lambda}$K and $^{48}_{\Lambda}$K measurements as E12-15-008.

We submitted to PAC 44 a new proposal on $^{40}_{\Lambda}$K and $^{48}_{\Lambda}$K, mainly focused on the isospin dependence of hyperon dynamics, which was approved.

In view of the astrophysical implications, valuable additional information can be obtained by expanding the kaon electroproduction program to include a study of the ^{208}Pb(e,e'K^+)$^{208}_{\Lambda}$Tl reaction.

Thanks to the extended region of constant density and the large neutron excess, ^{208}Pb provides the best available proxy of neutron star matter. Therefore, the use of a ^{208}Pb target will allow to investigate hypernuclear dynamics in a new environment, in which three-body interactions are expected to play an important role. In addition, the availability of accurate ^{208}Pb(e, e'p)^{207}Tl data will allow to exract the Λ binding energies from the measured (e,e'K^+) cross section using a largely model independent procedure. The results of this analysis will provide essential information, needed to constrain and improve the available models of YN and YNN potentials.

We submitted this proposal 2 years ago, it was deferred. This is an update version of it following the reccomendations given by the PAC

1. Introduction

The presence of hyperons (i.e. baryons with strange content) in finite and infinite nuclear systems constitutes a unique probe of the deep nuclear interior which gives us the opportunity to study baryon-baryon interactions from an enlarged perspective and to extend, in this way, our present knowledge of conventional nuclear physics to the SU(3)-flavor sector.

Contrary to the nucleon-nucleon (NN) interaction, which is fairly well known due to the large number of existing scattering data and measured properties of nuclei, hyperon-nucleon (YN) and hyperon-hyperon (YY) interactions are still poorly constrained. Owing to the severe difficulties involved in the

extraction of the potential describing YN interactions from YN scattering data, the study of hypernuclear spectroscopy appears to be the most effective approach to obtain new information.

In fact, one of the goals of hypernuclear physics is to study precisely, trough spectroscopic investigation of Λ hypernuclei (nuclear many-body systems containing one Λ particle), hypernuclear observables with the underlying bare hyperon-nucleon (YN) and hyperon-hyperon (YY) interactions.

Neutron stars, remnants of the gravitational collapse of massive stars, have masses and radii of the order of 1-2 $M_\odot$ ($M_\odot$ ~ 2 x10^{33}g being the mass of the Sun) and 10 - 12 km, respectively and central densities in the range of 4 - 8 times the normal nuclear matter saturation density, ε_o = 2.7 x 10^{14} g/cm^3 (ρo ~ 0.16 fm^{-3}). They are most likely among the densest objects in the Universe. These objects are an excellent observatory to test our present understanding of the theory of strong interacting matter at extreme conditions, and they offer an interesting interplay between nuclear processes and astrophysical observables. Conditions of matter inside neutron stars are very different from those one can find in Earth, therefore, a good knowledge of the Equation of State (EoS) of dense matter is required to understand the properties of these objects.

Nowadays, the true nature of neutron stars is still an open question. Traditionally the core of neutron stars has been modeled as a uniform fluid of neutron-rich nuclear matter in equilibrium with respect to the weak interaction (β-stable matter). Nevertheless, due to the large value of the density, new hadronic degrees of freedom are expected to appear in addition to nucleons. Hyperons are an example of these new degrees of freedom. Contrary to terrestial conditions, where hyperons are unstable and decay into nucleons through the weak interaction, the equilibrium conditions in neutron stars can make the inverse process happen. Hyperons may appear in the inner core of neutron stars at densities of about 2-3 ρo. At such densities, the nucleonic chemical potentetial is large enough to make the conversion of nucleons into hyperons energetically favorable making the EoS softer consequentely reducing the maximum mass.

This is in contrast with the astrophysics observations ("hyperon puzzle"). The solution of this problem isn't easy. A mechanism that could provide additional repulsion making EoS stiffer is needed.
Different mechanism have been proposed that could provide additional repulsion: a. exchange of vector meson, b. *repulsive three body forces*, c. phase transition to deconfined quark matter at densities below the hyperon threshold.

1. Proposed experiment

The JLab hypernuclear collaboration proposed to PAC43 a coherent series of studies of the (e,e'K$^+$) reaction, to be performed using targets spanning a wide range of mass. The purpose of this analysis was investigation of the ΛN interactions in a variety of nuclear media.

The collaboration submitted to PAC 44 a new proposal on $^{40}_{\Lambda}$K and $^{48}_{\Lambda}$K, mainly focused on the isospin dependence of ΛN interaction, which was approved.

Subsequently, a Letter Of Intent concerning the study of the reaction $^{208}Pb(e,e'K^+)^{208}_{\Lambda}Tl$ *has been submitted to PAC 45. The PAC encouraged the collaboration to submit the present proposal.*

The technique of (e,e′K$^+$) hypernuclear spectroscopy is currently the only method that can measure the absolute hypernuclear binding energy centroids for ground and excited states with an unprecedented accuracy of <100 keV. It should be noted that reaction spectroscopy such as (e,e′K$^+$) hypernuclear spectroscopy provides information on the cross section as well as on the binding energy. These information are complementary to the information obtained by decay product studies such as gamma and decay-pion spectroscopies.

A consistent theoretical framework for the analysis of electron-nucleus scattering in the impulse approximation regime—in which the nuclear cross section can be written in factorised form using the Green's function formalism—has been widely and successfully applied to the analysis of (e, e'p) data, see [Benhar2016]. The recent progresses in the treatment of both the elementary e + p → e' + Λ + K$^+$ reaction [Bydžovský2018] and the transition amplitues of heavy nuclei [Vidaña2017], will allow the generalisation of this approach to the description of the ^{208}Pb(e,e'K$^+$)$^{208}_{\Lambda}$Tl cross section [Benhar2020]. In addition, the

availability of accurate ^{208}Pb(e, e'p)^{207}Tl data will allow to exract the Λ binding energies from the measured (e,e'K$^+$) cross section using a largely model independent procedure. The results of this analysis will provide essential information, needed to constrain and improve the available models of YN and YNN potentials

2.1 Neutron stars and the Hyperon puzzle

Neutron stars (NS) are the most compact and dense stars in the universe, with typical masses $M \sim 1.4\, M_{\odot}$ and radii R~10 km. Their central densities can be several times larger than the nuclear saturation density, $\rho_0 = 0.16$ fm^{-3}. Since the Fermi energy of fermions at such densities is in excess of tens of MeV, thermal effects have little influence on the structure of NS. Therefore, they exhibit the properties of cold matter at extremely high densities, very far from being realized in present terrestrial experiments. In the era of multi-messenger astronomical observations, NS offers a unique opportunity to test a broad class of theories, from nuclear physics to general relativity, including the recent observation of gravitational waves.

From the surface to the interior of a NS, stellar matter undergoes a number of transitions. From electron and neutron-rich ions in the outer envelopes, the composition is believed to change into a degenerated gas of neutrons, protons, electrons and muons in the outer core.
At densities larger than ~$2\rho_0$ new hadronic degrees of freedom or exotic phases are likely to appear. Fig.2-1 shows the chemical potentials and concentrations of stellar constituents in beta-stable hyperonic matter as a function of baryon density, obtained from a recent theoretical calculation employing modern baryonic potentials [Bom16].

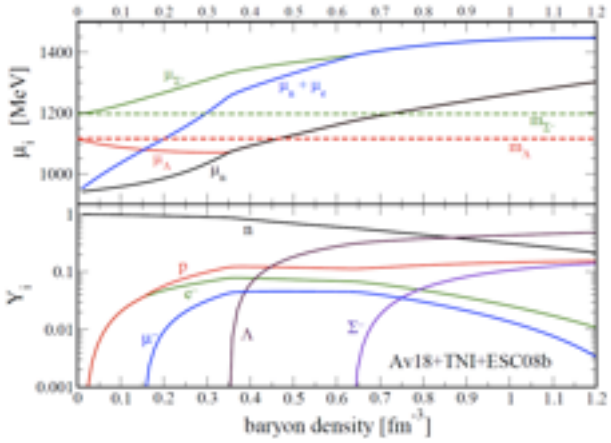

Figure 2-1: Chemical potentials μ, and concentrations Y of the stellar constituents in hyperonic matter as a function of the baryon density [Bom16].

The first theoretical indication for the appearance of hyperons in the core of a NS was already advocated in 1960 [AMB60]. In the degenerate dense matter forming the inner core of a NS, Pauli blocking would prevent hyperons from decaying by limiting the phase space available to nucleons. When the nucleon chemical potential is large enough, the conversion of nucleons into hyperons becomes energetically favorable. This results in a reduction of the Fermi pressure exerted by the baryons and a softening of the equation of state (EOS). As a consequence, the maximum mass determined by the equilibrium condition between gravitational and nuclear forces is reduced. The value of about $1.5M_{\odot}$ for the maximum mass of a NS, inferred from neutron star mass determinations [THO99], was considered the canonical limit, and it was compatible with most EOS of matter containing strangeness. However, the recent measurements of the large mass values of the millisecond pulsars J1614-2230 ($1.97(4)M_{\odot}$) [DEM10] and PSR J0348+0432 ($2.01(4)M_{\odot}$) [ANT13] require a much stiffer equation of state.

This seems to contradict the appearance of strange baryons in high-density matter given what is known at present about the hyperon-nucleon interaction. This apparent inconsistency between NS mass

observations and theoretical calculations is an outstanding problem, ß known as “hyperon puzzle”. Its solution will require a better understanding of the YN interaction in a wide range of systems, from light to medium and heavy hypernuclei, as well as the development of a consistent framework allowing for accurate theoretical calculation.

Currently there is no general agreement (even qualitative) among the predicted results for the EOS and the maximum mass of NS including hyperons. This has to be ascribed to the combination of an incomplete knowledge of the forces governing the system (in the hypernuclear case both two- and three-body forces), and to the concurrent use of approximated theoretical many-body techniques. Some classes of methods extended to the hyperonic sector predict the appearance of hyperons at around 2-3 ρ_0, and a strong softening of EOS, implying a sizable reduction of the maximum mass [VID11, HJS11, MAS12]. On the other hand, other approaches suggest much weaker effects arising from the presence of strange baryons in the core of the star [BED12, WEI12, MIY13, LOP14].

The large body of available nucleon-nucleon scattering data allows one to derive satisfactory models of two-body nuclear forces, either purely phenomenological [WIR95] or built on the basis of an effective field theory [MAC96, EPE05, EKS13, GEZ13]. In the hyperon-nucleon sector, few scattering data are available, although a ΣN scattering experiment is currently in preparation at J-PARC [MIW11], and no scattering data exist in the hyperon-hyperon sector. The main reasons of this lack of information lie in the instability of hyperons in the vacuum, and the impossibility of collecting hyperon-neutron and hyperon-hyperon scattering data. This implies that realistic hypernuclear interaction models must also rely on information extracted from the binding energies of hypernuclei.

In the non-strange nuclear sector the binding energies of light nuclei have been used to constrain three-nucleon potential models. However, the most accurate phenomenological three-body force (Illinois 7 [PIE08]), while providing a satisfactory description of the spectrum of light nuclei up to ^{12}C [PIE08] yields to a pathological EOS for pure neutron matter (PNM) [MAR13]. On the other hand, when additional information on the three-nucleon interaction is inferred from saturation properties of symmetric nuclear matter (Urbana IX force [PUD95]), the resulting PNM EOS turns out to be stiff enough to be compatible with astrophysical observations [GAN12]. Recent analysis of ^{16}O-^{16}O scattering data shows that the established meson exchange potential model (Nijmegen ESC08c [NAG14]) cannot reproduce the cross section at large scattering angles and inclusion of 3-body/4-body repulsive forces solves the problem [FUR09].

Thus, there is a general indication that 3-body/4-body repulsive forces become quite significant at high density, but they cannot be constrained from light systems. In a similar fashion, the binding energies of light hypernuclei do not suffice in constraining hypernuclear interactions. Heavier hypernuclei have been studied with pion beams but the achieved precision is not enough to extract detailed information about the 3-body hyperon-nucleon force.

Additional information must necessarily be inferred from the properties of medium and heavy hypernuclei in order to extrapolate to the infinite-mass limit for discussion of highly massive asymmetric nuclear matter such as neutron stars and strange hadronic matters (n_u~n_d~n_s).

The hypernuclei ^{40}□K and ^{48}□K, show very different isospin asymmetry (δ=0.05 and 0.188, respectively) that allows us to extract isospin dependence of the 3-body ΛNN force.

The approved proposal E12-15-008 will study this part.

Here, we propose a study of the $^{208}Pb(e,e'K^+)^{208}_{\Lambda}Tl$ reaction, in which the use of a much heavier target with large neutron excess, providing a good proxy of matter in the neutron star interior, is exploited to obtain complementary information on three-body forces, needed to address the “hyperon puzzle”. Note that in the non strange sector the contribution of three-nucleon forces, which is known to be large and repulsive in nuclear matter at equilibrium density, is believed to be much smaller and attractive in 40Ca [LONA2017].

The measured charge density distribution of ^{208}Pb, illustrated in Fig.2.2 [Fro], clearly shows that the region of nearly constant density accounts for a very large fraction (~70 %) of the nuclear volume, thus suggesting that its properties largely reflect those of uniform nuclear matter in the neutron star interior. The validity of this conjecture has been long established by a comparison between the results of theoretical

calculations and the data extracted from the ^{208}Pb(e,e′p)^{207}Tl cross sections measured at NIKHEF in the 1980s [Quint, Baten]

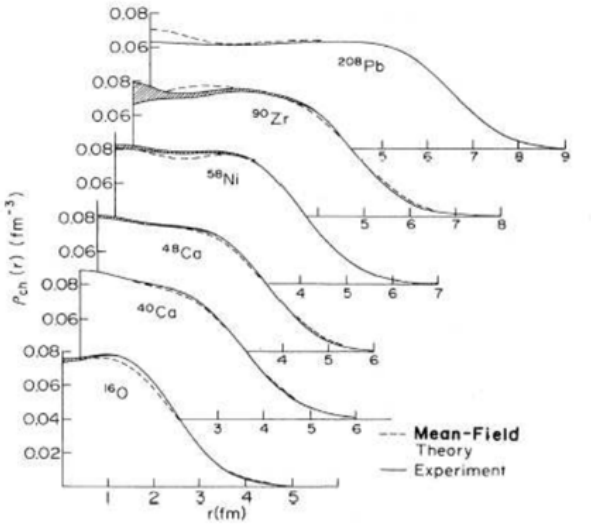

Fig. 2.2 Charge density distributions of nuclei with mass 16 ≤ A ≤ 208 [Fro]

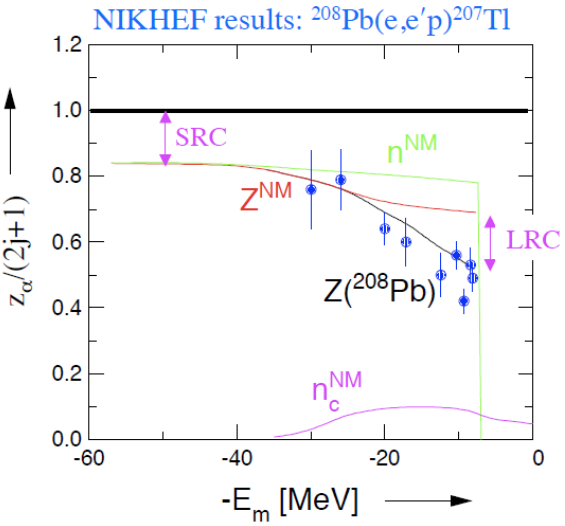

Fig. 2-3 Energy dependence of the spectroscopic factors extracted from the measured ^{208}Pb(e,e′p)^{207}Tl cross sections [BEN90, Quint, Baten] compared to the theoretical results of Ref. [BEN90]. The black and red solid lines, labelled Z(^{208}Pb) and Z^{NM}, correspond to ^{208}Pb and uniform nuclear matter, respectively. The effects of short- (SRC) and long-range-correlations (LRC), the latter arising from surface and shell effects, are indicated.

As shown in Fig. 2-3 the energy dependence of the spectroscopic factors, obtained from the analysis of the measured missing energy spectra, turns out to be in remarkably good agreement with the results reported in the pioneering work of Ref. [BEN90]. Short-range correlations appear to be the most important mechanism leading to the observed quenching of the spectroscopic factor, while surface and shell effects only play an important role in the vicinity of the Fermi surface.

The picture emerging from Fig. 2.3 suggests that deeply bound protons in the ^{208}Pb ground state largely behave as if they were in nuclear matter.

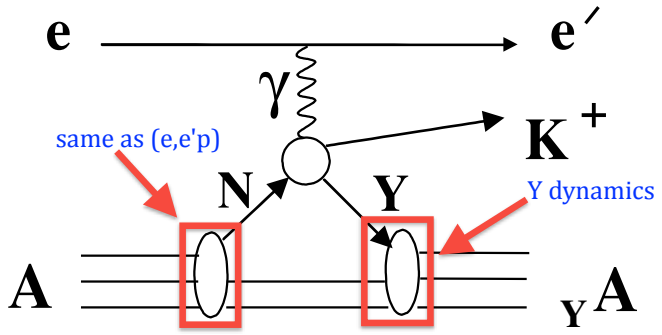

Fig. 2-4 Schematic representation of the (e,e´K^+) reaction. The left and right boxes highlight the amplitudes involved in the proton and Λ spectral functions, respectively

Figure 2-4, provides a schematic representation of the (e,e´K^+) reaction, illustrating the connection with the corresponding (e,e´p) process. The left and right boxes highlight the amplitudes determined by nuclear and hypernuclear dynamics described by the nucleon and hyperon spectral functions respectively.

The availability of the information obtained from the measured (e,e´p) cross sections will be critical for the interpretation of (e,e´K^+) data.

To see this, just consider that the hyperon binding energies are given by the difference between the missing energies measured in (e,e´K^+) and the proton binding energies obtained from the (e,e´p) cross sections.

Hence, (e,e´p) data will provide the baseline needed to extract information on hyperon binding energies.

The recent progresses in the treatment of both the elementary e + p → e' + Λ + K^+ reaction [Bydžovský2018] and the transition amplitues of heavy nuclei [BEN90,Vidaña2017], will allow the generalisation of the approach based on factorization, successfully employed to analyse (e, e'p) data, to the description of the ^{208}Pb(e,e'K^+)$^{208}_{\Lambda}$Tl cross section [Benhar2020]. The results of this analysis, combined with the availability of model independent information on the hyperon binding energies, will allow to constrain and improve the available models of YN and YNN potentials.

In view of the above considerations, the use of a ^{208}Pb target appears to be best suited to obtain information Λ interactions in a uniform nuclear medium with large neutron excess.

2.2 Theoretical models

A simple theoretical description of Λ–hypernuclei consists of an ordinary nucleus with a Λ sitting in one of the single-particle states of an effective Λ-nucleus mean field potential. In this description, whose quality relies on the validity of the mean field picture, the hypernuclear Hamiltonian consists of the Hamiltonian for the core-nucleus, the Λ kinetic energy and the sum of ΛN interaction terms that can be derived with various theoretical frameworks.

From the analysis of hypernuclear binding energies and the limited available YN scattering data, different baryon-baryon interaction models have been formulated. A commonly followed approach to construct YN and YY interactions is to start from a given nucleon-nucleon one and to extend it to the strange sector by imposing the SU(3)-flavor symmetry to fix all those parameters that cannot be fixed by the scarce amount of scattering data. This has been mainly done in the framework of a meson-exchange theory by the Nijmegen [MAE89,RIJ99,STO99,RIJ06,RIJ06b] and Juelich [HOL89,HAI05] groups. Recently, a new approach based on chiral effective field theory (CEFT) has emerged as poweful tool [POL06,HAI13,HAI20]. Microscopic hypernuclear structure calculations can provide the desired link between hypernuclear observables and the bare YN and YY interactions. These calculations are based on the construction of effective YN and YY interactions derived from the bare YN and YY ones by using diferents approaches such as G matrix methods. The most recent study of the structure of single-Λ hypernuclei from $^{5}_{\Lambda}$He to $^{209}_{\Lambda}$Pb based on a G-matrix method has employed chiral YN potentials of the Juelich-Bonn-Munich group [POL06,HAI13,HAI20] derived at leading order (LO) and next-to-leading order (NLO) [HAI20b]. A sizable cut-off regulator

dependence was found signaling that higher-order contributions in the chiral expansion, and specificaly three-body forces, have to play a non-negligible role in determining quantitatively the structure of heavy hypernuclei. CEFT establishes a prescription to extend the interaction model to include many-body forces. Performed next-to-leading order (NLO) calculations already included some components of the 3-body force (the ones that can be reduced to 2-body terms), but next-to-next-to-leading order (NNLO) calculations are necessary for the inclusion of a genuine 3-body interaction, and more experimental inputs are required to constraint the low-energy constants.

Recently, the auxiliary field diffusion Monte Carlo (AFDMC) technique for strange systems has made substantial progresses. By using this microscopic ab-initio approach, an accurate analysis of the Λ separation energy of light- and medium-heavy hypernuclei has been carried out [LON14, PED15] using a phenomenological interaction [BOD84, USM95, IMR14] in which the two-body potential has been fitted on the existing Λp scattering data. As shown in Fig. 2-4(a), when only the two-body ΛN force is considered (red curve), the calculated hyperon separation energies tend to disagree with the experimental data (green curve) as the density increases. The inclusion of the three-body ΛNN force in this scheme leads to a satisfactory description of the hyperon separation energies in a wide mass range and for the Λ occupying different single particle state orbitals (s, p and d wave), as shown in Figs. 2-5(b)

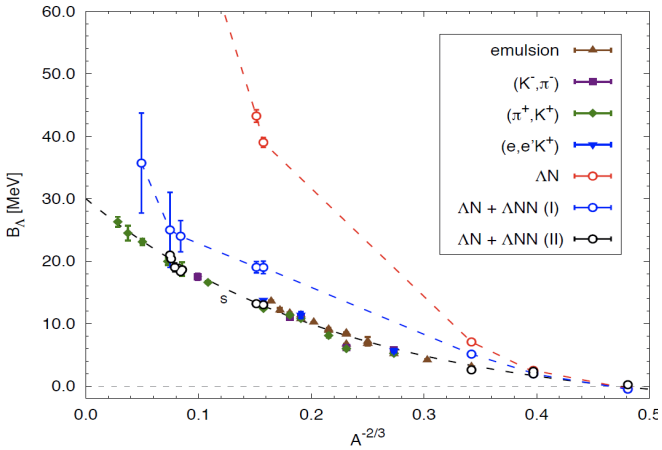

(a) Experimental B_Λ values in s wave and AFDMC calculation results with 2-body ΛN interaction alone, and two different parametrizations of the 3-body YN interaction (updated from [LON14]).

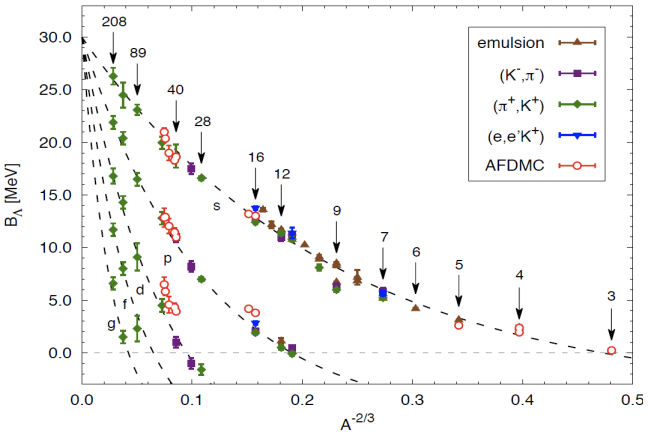

(b) Experimental results for Λ in s, p, d, f and g waves. Red open circles are the AFDMC results obtained including the most recent 2-body plus 3-body hyperon-nucleon phenomenological interaction model (updated from [PED15]).

Figure 2-5: Λ separation energies as a function of $A^{-2/3}$. Predicted results for $^{40}_{\Lambda}$K and $^{48}_{\Lambda}$K are also included.

However, these potential models predicting relatively small differences in the Λ separation energies of hypernuclei give dramatically different results as for the properties of the infinite medium [LON15]. The resulting EOS spans the whole regime extending from the appearance of a substantial fraction of hyperons at $\sim 2\rho_0 \simeq 0.32$ fm^{-3} to the absence of Λ particles in the entire density range of the star, as shown in Fig. 2-5(a). This has a sizable effect on the predicted NS structure, Fig. 2-6(b).

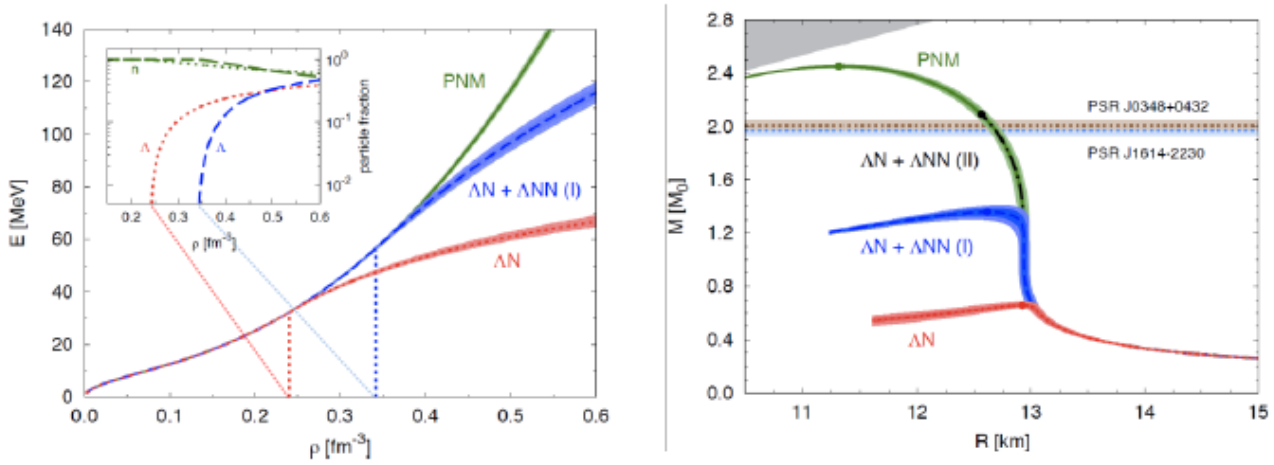

(a) Equations of state. The vertical dotted lines indicate the Λ threshold densities. In the inset, neutron and Λ fractions corresponds to the two hyper-neutron matter EOSs.

(b) Mass-radius relations given by AFDMC. Closed circles represent the predicted maximum masses. Horizontal bands at $2M_{\odot}$ are the observed masses of the heavy neutron stars [DEM10, ANT13].

Fig. 2-6 EOS and neutron star mass-radius relaytions calculated by AFMDC [LON15]

Other techniques such as G-matrix or AMD calculations employing multi-baryon interactions, for instance the the ESC08c+MPa potential, are able to reprocude B_{Λ} of a wide range of hypernuclei with accuracy of <1 MeV and similar result for EOS of neutron stars which can support 2 solar mass was obtained [YAM14, ISA16]. We note that very recently the effect of chiral hyperonic three-body forces on neutron stars and hypernuclei has been analyzed within the Brueckner theory [LOG19]. The results of this work show that the inclusion of a moderately repulsive NNΛ force leads to an EOS stiff enough such that the resulting neutron star maximum mass is compatible with the largest currently observed values being the hyperon fraction in the interior of the star non-negligible. This work shows also that the agreement between the calculated L separation energies of heavy hypernuclei such as $^{90}_{\Lambda}$Zr and $^{209}_{\Lambda}$Pb and the experimental data improves when the effect of the NNΛ force is taken into account. Being its repulsive contribution of this force of about 10 MeV.

Although these calculations are based on different theoretical techniques and different baryonic potential models, they all predict a similar tendency of repulsive three-body forces at high density, suggesting a possibility to make the EOS of hyper-nuclear matter hard enough to support 2 solar mass neutron stars.

However, while 2-body baryonic force models based on different theoretical frameworks are reasonably accurate, detailed information on the hyperonoic three-body forces is still missing. In particular very little is known on the isospin dependence of such multi-baryon forces, which plays a crucial role in the determination of the structure of neutron stars.

This lack of knowledge is to be attributed to a poor experimental information for medium-heavy neutron-rich hypernuclei, which are the key to infer properties of the infinite hyper-nuclear matter.

Therefore, in order to properly assess the role of hyperons in NSs and reconcile theoretical predictions with astrophysical observations, *i.e.* solve the hyperon puzzle, precise experimental investigation on medium-heavy neutron-rich targets is of paramount importance and only JLab can provide such an accurate experimental data.

2.3 Spectroscopy of ^{208}Pb hypernucleus

The study of the medium – heavy mass hypernuclei is particulary interesting. However, present experimental information in this mass region relies uniquely on the data measured by the (π^+,K^+) reaction.

The resolution as well as absolute energy scale calibration of the (π^+, K^+) data are no satisfactory. Data in the A = 40 mass region will be collected by the approved E12-15-008 experiment.

The clean extraction of Λ single-particle from (π^+,K^+) or (e,e'K^+) reactions require a filled shell of high-j neutrons or protons, respectively, near the Fermi surface. This is because the cross section is proportional to the number of nucleons in the shell. The high momentum (angular momentum) transfer permits the population of all bound Λ orbits with a wide range of orbital angular momentum values.

Closed shells for the other kind of nucleon makes for maximal symplicity of the level structure and the observed spectrum. Thus, the obvious choice for the heaviest target is the doubly-magic ^{208}Pb nucleus.

Moreover data from (π,K) as well as from several (e,e'p) experiments exists [HASHI, Quint, Baten, Bobel]. In addition, it should be noted that the Λ-N particle-hole matrix elements are very small for heavy nuclei and that the level shifts and redistribution of strength due to configuration mixing will not lead to observable effects, even with the good resolution possible for the (e,e'K) reaction.

New microscopic calculation are available [LON14,LON15, BENA1]**.** *These calculations show that the inclusion of explicit ΛNN terms provides the necessary repulsion to realistically describe the separation energy of a Λ in hypernucley of intermediate and high masses [LON14,LON15]. They showed that failing to simultaneously reproduce all the experimental separation energies, thus suggesting that three-body interactions involving nucleons and hyperons may have sizable effects*

Combining the results of the AFDMC studies and the existing models of the ^{208}Pb spectral function, the formalism successfully employed to describe the (e,e'p) cross section can be readily generalized to the case of Λ electroproduction[BEN90].

^{208}Pb was studied using the (π^+, K^+) reaction and the shell structures were barely visible [HASHI]. The main reason was poor resolution (> 2MeV FWHM). This resolution is larger than the 1.8 MeV spacing between the 0i13/2 and 0h9/2 neutron hole states that produce two series of strongly populated states with the Λ in different orbits. In addition, the spacing between Λ single-particle states is only 4 to 6 MeV. As a result, the existing data do not resolve the two series of states, introducing uncertainties into the theoretical analyses.

The experiment we propose can have good statistics and sufficient resolution to separate at least the major shell states from those configuration mixing states as seen in the Hall C ^{28}ΛAl spectrum [NAKA, HASHI2010, TANG115].

The study of ^{208}Pb with the (e, e'K^+) reaction will give better resolution and thus a more detailed understanding of baryon behavior deep inside of the nucleus.

The more accurate information on the binding energies and spacing of the Λ single-particle states in heavy nuclei will provide an anchor point for the systematics of Λ single-particle states across the periodic table.

Moreover, ^{208}Pb is the ideal target to study hyperons in a medium closely resembling neutron star matter. This environment is best suited to the investigate the effects of three body forces involving hyperons[LON14,LON15, SHARMA, BOBEL] which increase the stiffness of the nuclear matter equation of state, thus allowing for the existence of massive neutron stars compatible with the observational constraints.

As pointed out in the introduction, hyperon production in the neutron star interior is believed to become energetically favored at around 2-3 times nuclear saturation density, and its occurrence may also signal the presence of a non-hadronic phase, i.e. of deconfined quark matter, in the inner core of the star.

In conclusion, even if the typical baryon density inside a neutron star is much higher than in a hypernucleus a precise knowledge of the ^{208}Pb level structure can, by constraining the hyperon-nucleon potential, contribute to more reliable predictions regarding the internal structure of neutrons stars, and in particular their maximum mass.

2.3.1 Proposed measurement

The aim of the experiment is measuring the ^{208}Pb(e,e'k)^{208}Tl reaction. Fig 2.7 a shows the missing mass spectrum obtained by the ^{208}Pb (π,K)^{208}ΛPb experiment [Hasega]. It shows a characteristic bump structure starting from the binding energies BΛ around 25 MeV. As explained in the previous section, two

series of states with the Λ hyperon coupled to the high-j neutron hole states near the Fermi surface are expected to be strongly populated but cannot be completely resolved. The binding energies of Λ hyperons were derived assuming they correspond to the peak centroids of the bumps. Although the binding energies may depend on detail of the bump structures, the centroid values can be reasonably well deduced form the fitting [Hasega]. Binding energy have been measured with the same reaction in several other nuclei, light and medium mass [HASHI] to study its mass dependence also to get information about the distinguishability of the Λ hyperon in the nucleus [DOVER].

The observed spectra were found to be significantly smoother than theoretical calculations [HASHI, Hasega]. "Therefore is of vital importance to perform precision spectroscopy of heavy Λ hypenuclei with mass resolution comparable to or better than the energy differences of core excited states, in order to further investigate the structure of the Λ hyperon deeply bound states in heavier nuclei. (e,e'K) spectroscopy is a promising approach to this problem"[HASHI].

Spectroscopic data exist for few Λ hypernuclei also for (e,e'K) spectroscopy and few others would be available with the presently proposed experiment on $^{40}_{\Lambda}$K and $^{48}_{\Lambda}$K.. Consequently is extremely important to perform (e,e'K) experiment also on ^{208}Pb. The much better energy resolution of the (e,e'K), a factor of ~ 3 with respect to (π,K), will allow much more precise Λ single-particle energies to be determined.

It will be possible to "see" deep shells, in practice not visible with (π^+,K^+) reaction ("the observed small peaks are assumed to be the sΛ states" [Hasega])

This will make possible to determine with much better precision the binding energy (also for the possibility of calibration with hydrogen), and to test different theoretical models: relativistic mean field calculations, *calculations using three-body ΛNN forces* and Λ effective mass in the Skyrme Hartree Fock approach [YAMA, YAMA1], the new microscopic MonteCarlo calculations [LON14,LON15]) and other many body calculations [BENA1]

This will allow us to extend the A range in the study of the mass dependence of the Λ binding energy.

Measurements of the Λ binding energy have been already performed with the (e,e'K) reaction in Hall A and Hall C reaction on several nuclei including the nominally doubly-closed shell nucleus ^{16}O. Moreover, as previously mentioned, an experiment on $^{40}_{\Lambda}$K and $^{48}_{\Lambda}$K has already approved by the Jlab PAC

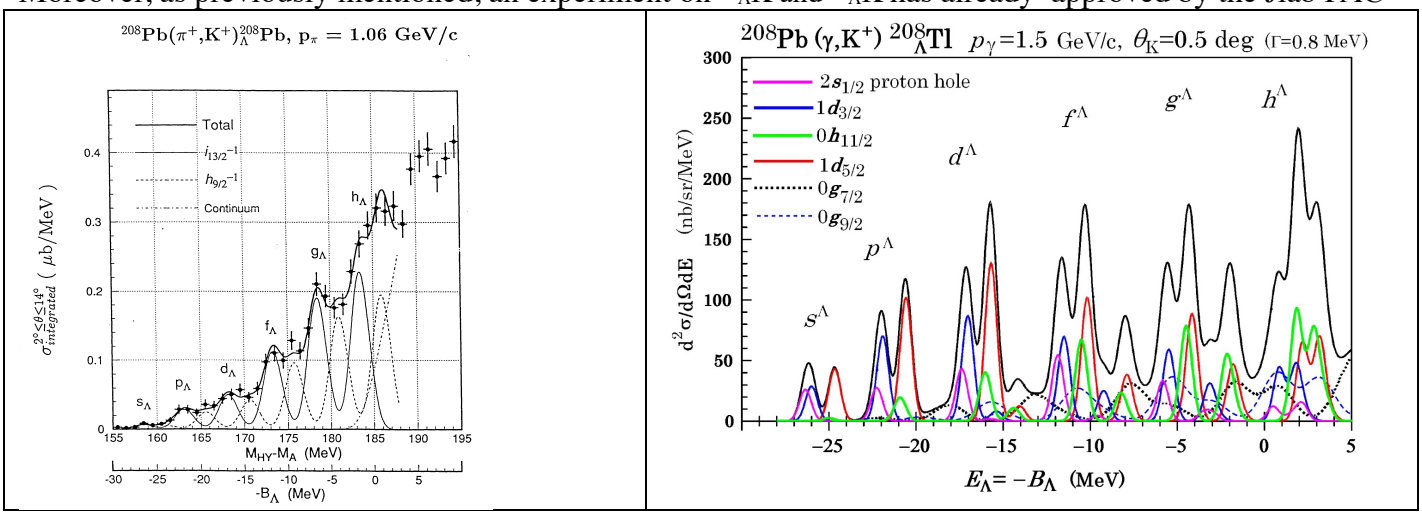

a b

Fig. 2.7. a. Missing mass spectrum of $^{40}_{\Lambda}$K and $^{48}_{\Lambda}$K measured in the E140 experiment. b $^{207}_{\Lambda}$Tl core nucleus level scheme

Fig. 2.8 shows the ^{208}Tl core nucleus level scheme and the spectroscopic factors measured in ^{208}Pb(d,3He)^{207}Tl reaction that are large enough to allow to see that many low-lying states of ^{207}Tl core nucleus (up to excitation energy approx. 4 MeV) and that the corresponding hypernuclear states with Λ coupled to these core states are populated.

Fig. 2.7 shows Spectrum for ^{208}Pb(γ,K+)$^{208}_{\Lambda}$ Tl calculated for our kinematics using the Saclay Lyon [SLA] elementary amplitudes. The Λ is assumed to be weakly coupled to the proton-hole states of ^{207}Tl strongly populated in (e,e'p) or (d,3He) reactions on ^{208}Pb. The Λ single-particle energies were calculated from a Woods-Saxon well fitted to energies derived from the $^{208}_{\Lambda}Pb(\pi^+,K^+)^{208}_{\Lambda}Pb$ reaction.
States based on the closely-spaced 2s1/2^{-1} and p 1d3/2^{-1} states cannot be resolved (blue bars and curves).

Likewise for the p 0h11/2^{-1} and p 1d5/2^{-1} states cannot be resolved (blue bars and curves). Likewise for the p 0h11/2^{-1} and p 1d5/2^{-1} states (red bars and curves). The successive red and blue peaks correspond to the population of the 0s, 0p, 0d, 0f, 0g, and 0h Lambda orbits.

The green lines correspond to the noded 1s, 1p, 1d/2s, and 1f Λ orbits. The remaining (wiggley) curves correspond to strength based on deeper and fragmented proton-hole strength

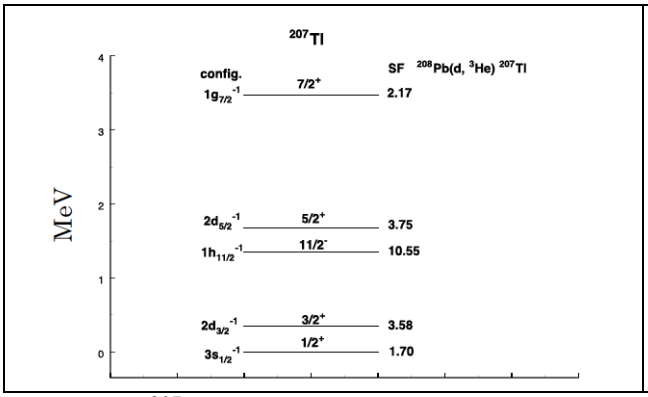

E_x MeV	J^π	Config.	C^2S
0.000	1/2+	$2s^{-1}_{1/2}$	1.70
0.351	3/2+	$1d^{-1}_{3/2}$	3.58
1.348	11/2−	$0h^{-1}_{11/2}$	10.6
1.683	5/2+	$1d^{-1}_{5/2}$	3.75
—	—	—	—
3.747	7/2+	$0g^{-1}_{7/2}$	2.17

Fig. 2.8 ^{207}Tl energy spectrum, dominant configurations and spectroscopic factors

Earlier, it was noted that in the standard shell-model framework configuration mixing effects should be small and not produce observable effects in the spectrum obtained with a Pb target. The Motoba/Millener calculation shown in Fig.2.7 b assumed weak-coupling of the Λ hyperon to the hole states of the core (i.e. no residual Λ–N interaction). This assumption can be checked by doing a simple particle-hole calculation with the Λ–N interaction that has been successful in describing the precision gamma-ray data obtained for p-shell hypernuclei. Then, one can extract Λ single-particle energies from each of the observed peaks. Each peak does correspond to several levels based on two closely-spaced proton-hole states. The fact that one should get essentially the same energies from the peaks based on the two sets of pairs of hole states, separated by 1 MeV, provides a check on the assumptions made.

It is also important to point out that, in the case of Pb target, a model independent determination of the spectrum can be obtained exploiting the availability of high resolution (e,e'p) data, providing the cbaseline for the interpretation of the measured missing energy spectra.

In the figures 2.9a, 2.9b, 2.9 c (with three possible energy resolutions, 600 kev, 800 kev, 1000 keV) we summarize the theoretical estimate, by T. Motoba, of the DWIA cross sections calculated at p(γ)= 1.5 GeV/c and θ(K)=0.5 deg, in which the Saclay-Lyon A amplitudes and the nuclear HO wave functions are employed (see also the summary table below). In drawing the spectra, however, the Λ single-particle energies from the Woods-Saxon potential are used instead of HO ones so as to be more realistic: E(Λ)=-25.99MeV(0s), -21.90(0p), -17.02(0d), -15.38(1s), -11.50(0f), -9.22(1p), -5.48(0g), -3.14(1d), -2.58(2s), +0.86(0h), +1.84(1f), +2.50(2p).

On the other hand, the proton single-hole energies are taken from the observed level energies of 207Tl: Ex=0.0 MeV (2s1/2^hole), 0.351MeV (1d3/2^), 1.348MeV (h11/2^), 1.682MeV (1d5/2^), 4.18MeV(approx. centroid of 0g7/2^), and 6.57MeV (no observed value, but centroid assumed for 0g9/2). Note that the spreading widths of 2 MeV are assumed to take account of the fragmented proton 0g7/2 and 0g9/2 orbits.

DWIA Cross Sections (nb/sr) for ^{208}Pb$(\gamma,K^+)^{208}_{\Lambda}$Tl at p_γ =1.5GeV/c and θ_K=0.5 deg.

	s^Λ	p^Λ	d^Λ		f^Λ	
Core state $(E_x) \times (nlj)^\Lambda$	$0s^\Lambda_{1/2}$	$0p^\Lambda_{3/2}$+$0p^\Lambda_{1/2}$	$0d^\Lambda_{5/2}$+$0d^\Lambda_{3/2}$	$1s^\Lambda_{1/2}$	$0f^\Lambda_{7/2}$+$0f^\Lambda_{5/2}$	$1p^\Lambda_{3/2}$+$1p^\Lambda_{1/2}$
$1/2^+(E_x$=0.0): $\pi(2s^{-1}_{1/2})$	22.2	15.6+ 7.8	22.1+14.8	1.6	26.6+20.0	2.6+1.3
$3/2^+(0.351)$: $\pi(1d^{-1}_{3/2})$	24.4	46.4+13.4	52.4+21.6	7.1	41.0+18.4	15.8+5.6
Left peak $d\sigma/d\Omega$	46.6	83.2	110.9	9.7	106.0	25.3
$(E_\Lambda = -B_\Lambda$ in MeV)	(−26.16)	(−21.97)	(−17.11)		(−11.64)	
$11/2^-(1.348)$: $\pi(0h^{-1}_{11/2})$	2.1	10.6+6.1	18.7+15.6	9.3	29.9+27.4	12.8+7.0
$5/2^+(1.682)$: $\pi(1d^{-1}_{5/2})$	36.7	51.7+35.2	58.1+52.4	10.6	42.9+44.0	20.3+12.4
Right peak $d\sigma/d\Omega$	39.8	103.5	144.8	19.9	149.3	52.5
$(E_\Lambda = -B_\Lambda$ in MeV)	(−24.70)	(−20.60)	(−15.74)		(−10.32)	(−7.96)

Figures 2.9(a,b,c) shows a series of doublet peaks indicated respectively by s^Λ, p^Λ, d^Λ, f^Λ, etc. As known from the energy differences between low-lying energy levels of ^{207}Tl, the proton-hole states are classified into two nearly degenerate groups in view of the `critical' value $\Delta Ex \simeq 0.35$ MeV. The left member of each doublet is attributed to the structure [core(1/2+, 3/2+) x $(nlj)^\Lambda$, while the right member to [core(11/2$^-$, 5/2$^+$) X $(nlj)^\Lambda$]. In the present calculation the elementary amplitude from the Saclay-Lyon model A is eployed, but it should be noted that SLA leads to considerable overestimate at very forward angle θLab $K \lesssim 5$ deg when compared with other theoretical models and/or experimental behaviors ($p \simeq 1.3$ GeV/c).
The upper plots are without the quasi free continuoum, the botton ones are with the quasi free.

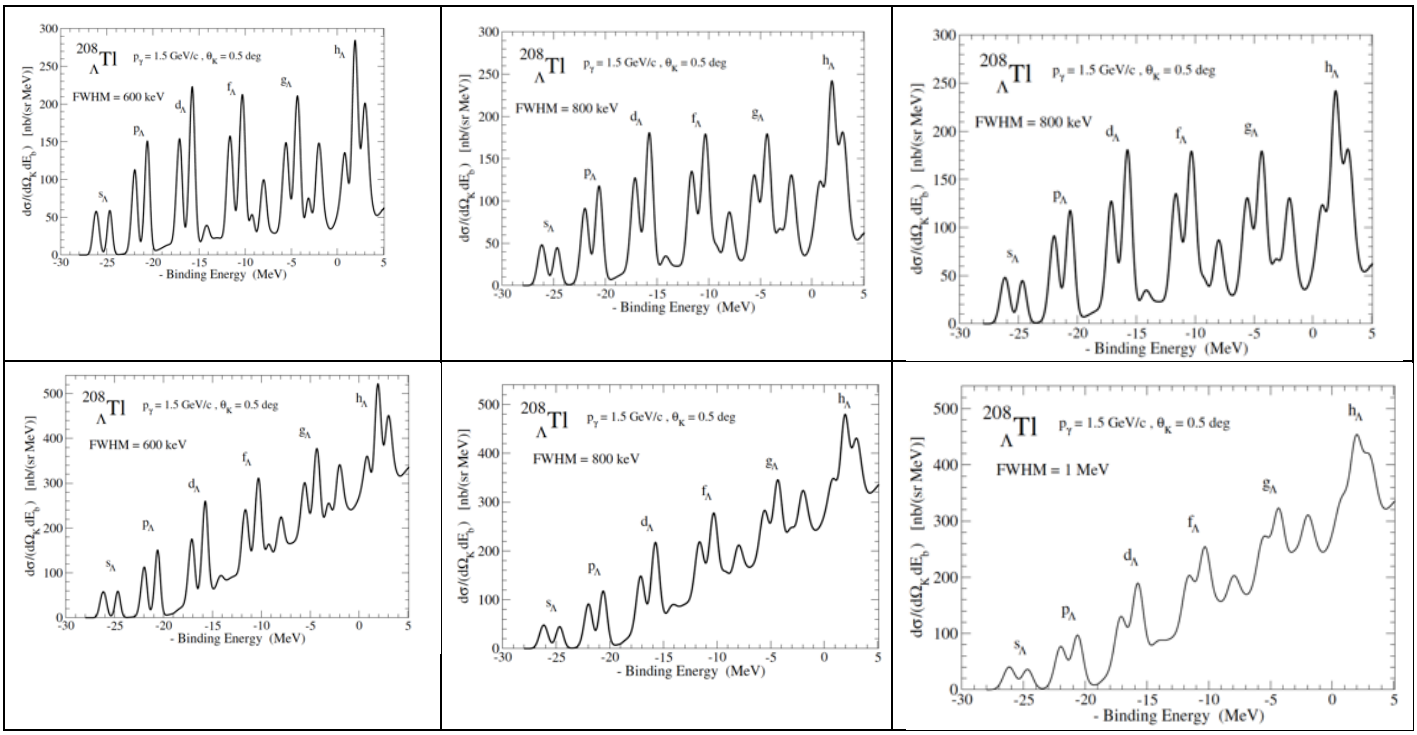

Fig. 2.9a Fig 2.9b Fig 2.9c

The cross section estimates suffer for incertitude due to input from the elementary process that cannot be determined more precisely due to the lack of data at kinematics of this proposal [Bydzovsky2012]. The presented calculations were done with the SLA model which predicts a steep decrease of the elementary cross section at very small kaon angles contrary to other models that predict a plateau or even increasing angular dependence at 1.5 GeV. Therefore one may expect that realistic values of the hypernucleus cross sections are smaller than those presented here.

3.Experimental Setup

3.1 Experimental configuration

The proposed experiment is to obtain high precision mass spectroscopy of the hypernucleus $^{208}_{\Lambda}Tl$ produced by the $^{208}Pb(\gamma, K^+)^{208}_{\Lambda}Tl$ reaction and will employ the same configuration of the experiment E12-15-008, already approved by JLab PAC, including a pair of room temperature Septum magnets, the high resolution HRS (Hall A) and the large solid-angle HKS spectrometers, as schematically illustrated in Fig. 3-1.

This pair of Separatiopn dipole magnets (PCS see later in the text) will be used to separate the scattered electrons and electro-produced kaons at small forward angles to sufficiently large spectrometer angles, while allowing the post-beam to be directly transported to the dump. It also minimizes the chance for the high rate backgrounds (electrons and positrons) at near zero degrees to enter either of the two spectrometers. The collaboration has demonstrated the technique successful in avoiding the background from e′ and K+ accidental coincidences by maintaining sufficiently low singles rates at each of the two spectrometers under high luminosity conditions.

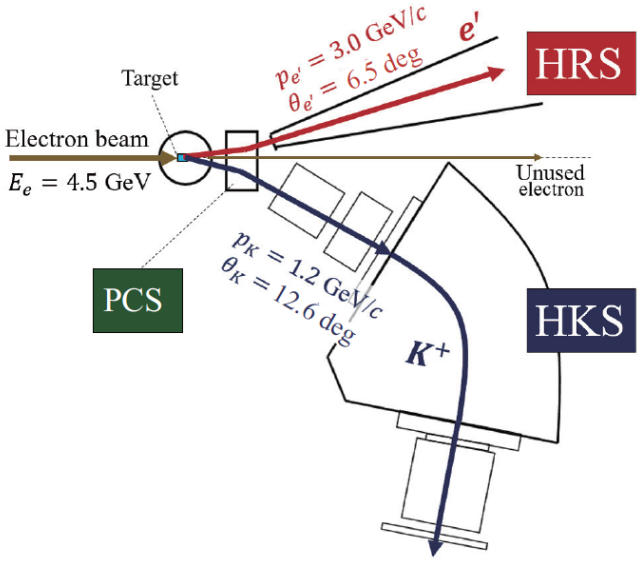

Figure 3-1: Schematic illustration of the experimental layout. A pair of Septum magnets will be used to separate the scattered electrons (analyzed by HRS) and the reaction kaons (analyzed by HKS).

One of the Hall A HRS spectrometer will be used to detect and analyze the scattered electrons with a momentum resolution of ~10^{-4} (FWHM) that is crucial to the overall energy resolution for the experiment

The HKS spectrometer that was successfully used in the previous Hall C experiments will be used as the kaon spectrometer. It features both a momentum resolution of ~$2x10^{-4}$.(FWHM) and a large solid angle acceptance that is three times larger than that of HRS. Its application is one of the important factors in achieving both high resolution and high yield in order to study spectroscopy of heavy hypernuclei. Its excellent detector system further cleanly identifies kaons.

One single target chamber will be used for all the planned targets including those to be used for calibrations. The entire system is vacuum connected.

Overall, this experimental design is for (1) the highest possible resolution (~800 keV FWHM in the case of Pb target, (2) the highest reachable yield, and (3) the lowest ever achievable background in electro-production of hypernuclei. Both involved spectrometers are well known and used previously with standard detector systems. The only new pieces of equipments are the separation dipole magnets (PCS) and the target

3.2 Beam

We are requesting a 25 μA beam at *Ee* = 4.5 GeV (two passes) with a bunch frequency of 500 MHz (250 MHz repetition rate will result in worse accidental background rate though it is still acceptable). In order to achieve a sufficient precision in a resulting missing-mass spectrum, the beam energy spread and energy centroid are required to be $\Delta p/p <= 5 * 10^{-5}$ (FWHM). A beam raster with an area of about (3 * 3 mm^2) need to be applied to avoid a damage on a target cell due to an overheat

3.3 Kinematics

The proposed kinematics is based on the use of a beam energy of E = 4.5238 GeV, the minimum HRS angle available when using a Septum for an e' central momentum of ~3 GeV/*c*, and a maximized overlap of the virtual photon angular range to the HKS angular acceptance in order to obtain the highest possible production yield. The kinematics parameters and ranges are listed in the Table below. With this kinematics, both the spectrometers are located at sufficiently large angles with respect to the beam to avoid the forward scattered electrons and positrons

Basic parameters for the present experiment

Beam	$\Delta p/p$	$< 1 \times 10^{-4}$ FWHM
	E_e	4.5 GeV
PCS + HRS (e')	D(PCS) + QQDQ	
	$\Delta p/p$	2.6×10^{-4} FWHM
	$p_{e'}$	3.0 GeV/$c \pm 4.5\%$
	$\theta_{ee'}$	6.5 ± 1.5 deg
	Solid angle $\Omega_{e'}$	2.4 msr
PCS + HKS (K^+)	D(PCS) + QQD	
	$\Delta p/p$	4.2×10^{-4} FWHM
	p_K	1.2 GeV/$c \pm 10\%$
	θ_{eK}	12.6 ± 4.5 deg
	Solid angle Ω_K	7 msr
	Optical length	12 m
	K^+ survival ratio	26%

A GEANT simulation taking into account the realistic and known conditions of both the HRS and HKS was performed

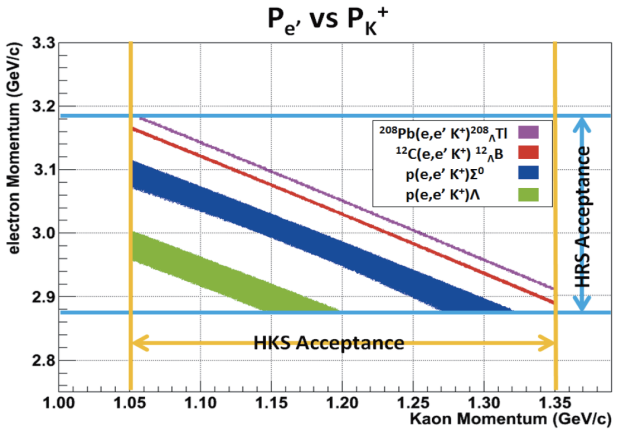

Fig. 3.2 Mass correlation in two dimensional momentum acceptance

3.4 Magnetic spectrometer

We request to use the exactly same spectrometer setup as the E12-15-008 experiment in which the isospin dependence of the LN/LNN interactions will be investigated through the 40,48Ca(*e,e'K+)* 40,48K reaction [42]. Existing spectrometers, HRS-L and HKS, combined with a new pair of charge separation dipole magnets (PCS) will be used for *e'* and *K*+ detection.

Construction and an excitation test of PCS has been completed in a Japanese company TOKIN in March 2020. More detailed measurement of magnetic field of PCS was carried out in XXXX 2020, and PCS is now ready for transport to JLab. Central momenta of HRS and HKS are set to be respectively 3.0 and 1.2 GeV/c, and the system covers a kinematical region of the reaction 208Pb(e,e'k) as shown in Fig. 3.2

Fig. 3-2 is an illustration of the e' and K^+ momentum correlation for various mass of hyperons (Λ and Σ^0) and ground state hypernuclei ($^{12}_{\Lambda}$B and $^{208}_{\Lambda}$Tl). The broadening of Λ and Σ^0 is from the range of recoil angles. Free Λ and Σ^0 productions are important for calibration of the absolute missing mass scale. In fact Λ and Σ_0, will be used for an absolute energy calibration. They will be measured with the same spectrometer setting for physics run thanks to the large momentum coverage of HKS ($\Delta p=p_{central} > 10\%$). Measuring both Λ and Σ_0 masses without a change of spectrometer setting minimizes a systematic error on B_Λ. Another important feature of HKS is a short path length. The path length of PCS + HKS is about 12 m, and thus 26% of *K*+s survive at 1.2 GeV/*c*. This gains a yield of Lambda hypernuclei by a factor of more than three compared to the (PCS+) HRS spectrometer in which *K*+s travel more than 23.4 m to be detected.

3.4 Spectrometer calibrations

Calibration of the spectrometer system is extremely important for the experiment to achieve its goal of high precision in determining the absolute mass (or Λ binding energy) and mass resolution. Standardized calibration methods and procedures successfully developed in the previous experiments will be applied again. A significant advantage of the new configuration is that these methods and procedures become more straight forward and can further improve the precision with much less analysis effort. This is because the two spectrometers are almost optically decoupled and there will be less information entanglement in the calibration data.

Some of light solid targets will be used for calibration as well as for precise determination of B_Λ. From experiences of previous hypernuclear programs at JLab, we learned that data for various solid targets with different energy loss contributions are quite useful to tune the backward matrix. We are considering using well studied CH_2, ^{10,11}B, ^{6,7}Li, ^{12}C targets for this purpose.

A thin CH_2 target will be used as part of overall calibration. Simultaneous production of Λ and Σ^0 particles from CH_2 is important in calibrating the precise absolute mass scale. (see Tab VI)

3.5 The ^{208}Pb target

A major concern of the collaboration is the development of a Pb target that could operate at up to 25 μA beam current without melting. The proposal requires a bare ^{208}Pb target with 0.1 mm thickness in beam. Pb is a challenge to develop as a target for electron beams because its thermal conductivity coefficient is about an order of magnitude smaller than Cu's at room temperature and its melting point, at 601 K, is very low.

There are three mechanisms through which a target could dissipate the heat deposited by the beam in it: conduction, convection and thermal radiation. Convection is ruled out since the target has to be inside a vacuum chamber. For a Pb target thermal heating radiation would dissipate at most a few percent of the total heat deposited in it, leaving conduction as the only viable thermal dissipation mechanism with a heat sink or forced cooling. For a given Pb target geometry cryogenic cooling can accommodate twice the beam current compared with room temperature cooling (typically with water). Another factor of two in beam current could be accommodated by rotating a cryogenically cooled Pb target in beam compared with a static one

We considered the setup used at NIKHEF for the (e,e'p) experiment [Bobel, Marchand].

This choice would allow us to run safely with 10 μA of beam current and 100 mg/cm2 of pure ^{208}Pb target cooled by water flow (15 °C) up to 95 dm^3/h during the data taking. In fact heat transfer calculation show that , for thick targets, conduction cooling becomes competitive as compared to increased radiation cooling by rotating or wobbling the target for thick targets. There are three mechanisms through which a target could dissipate the heat deposited by the beam in it: conduction, convection and thermal radiation. Convection is ruled out since the target has to be inside a vacuum chamber.

For a Pb target thermal heating radiation would dissipate at most a few percent of the total heat deposited in it, leaving conduction as the only viable thermal dissipation mechanism with a heat sink or forced cooling.

The computed temperature profile caused by a beam spot of radius r_0 on a circular target of radius r_1 is shown in Fig. 3.3.

The maximum current one can use without melting the target can be calculated by the formula

$$< i_{max}> = 2\pi k\ (T_{melting} - T_0)/\{[\ln(r_1/r_0) + ½]\ \rho dE/dx\}$$

where <i> is the beam current, k~ 35.3W.K^{-1}.m^{-1}, ρ~11.35 g/cm^{-3} for lead, $T_{melting}$ is 601 K for lead.

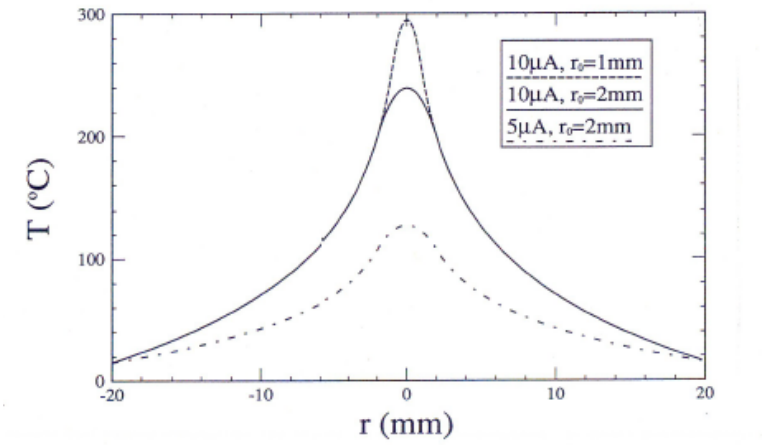

Fig.3.3. Temperature profile of a circular water cooled lead target of radius 20 mm. The dashed curve corresponds to 10 μA beam spot of 1 mm radius, the solid curve to a 10 μA beam spot of 2 mm radius. And the dot-dashed curve to a 5 μA beam spot of 2 mm radius.

We underline we will run with a 3 x3 mm2 rastered beam

What shown in the Fig. 3.3 gives only a first order estimation of the expected heat dissipation performance. For this reason we assume, conservatively, that we can run with 25 μA.

In fact for a given Pb target geometry cryogenic cooling can accommodate at least twice the beam current compared with room temperature cooling (typically with water). Another factor of two in beam current could be accommodated by rotating a cryogenically cooled Pb target in beam compared with a static one. But we are not going to rotate the target

The heating power deposited by a 25 μA electron beam current into a 0.1 mm thick Pb target would be about 5 W. Previously at least two Pb targets have been successfully designed and operated in electron beams at comparable beam heating powers: a Pb target operated at NIKHEF in the 1990s and the Pb target for the PREX2 experiment in Hall A at Jefferson Lab that completed its run in the fall of 2019. The NIKHEF target [BOBELDIJK] was water cooled bare ^{208}Pb target with a total thickness of 80 μm in beam that ran at an average beam current of 10 μA and 487 MeV energy. A report on this water-cooled target [MARCHAND] estimated a maximum beam current of 10 μA.

The PREX2 target had 10 separate ^{208}Pb foils, each about 550 μm thick in beam, sandwiched between two diamond foils, each 250 μm thick, mounted into a Cu frame and cryogenically cooled to 14 K

with cold He gas from the ESR as can be seen in Fig. 3.4, right. The target motion system allowed the positioning of a single sandwich C-Pb-C on the beam line at a time. The electron beam energy was 950 MeV. The PREX2 targets were run with beam currents of 70-85 μA and the beam rastered area on the target was 16-24 mm^2. PREX2 accumulated about 116 C of charge from six of the ten Pb targets. On average the lifetime of a target sandwich C-Pb-C in beam was estimated to be 20 C. The PREX2 target was designed by CFDFAC for beam currents up to 100 μA with a minimum beam raster area of 16 mm^2. The artificial diamond foils used in PREX2 had a thermal conductivity coefficient of at least 1000 W/m·K before beam operations. CFDFAC simulations showed that the lifetime of a sandwich C-Pb-C target heated by a 100 μA beam should be infinite if the diamond thermal conductivity is more than 300 W/m·K. If the diamond's thermal conductivity decreases below 100 W/m·K then the Pb foil in the sandwich can melt and the target is rendered out of commission. Radiation damage and direct beam exposure (thermal stresses) seem to be the main factors that contribute to an artificial diamond foil's degradation. CFDFAC made a thorough thermal assessment in the design of the PREX2 target. Four cooling agents were considered: liquid helium (LHe at 4.5 K), cold helium gas (GHe at 15K), liquid nitrogen (LN2 at 77 K) and cold nitrogen gas (GN2 at 78 K). Either kind of nitrogen cooling was shown to reduce significantly the lifetime of a target's sandwich in beam while the LHe cooling was shown to increase it by a small amount, so PREX2 chose GHe as coolant for its target.

A prototype Pb target for this experiment has been simulated at CFDFAC. The target consists of a bare ^{208}Pb foil 100 μm thick, mounted into the PREX2 Cu frame. Beam currents of 20 μA and 25 μA and coolant LHe (at 4.5 K) and GHe (at 14 K) respectively were considered. The geometry of the target is shown in Fig. 3.4. A summary of the CDF results is shown in Fig 3.5

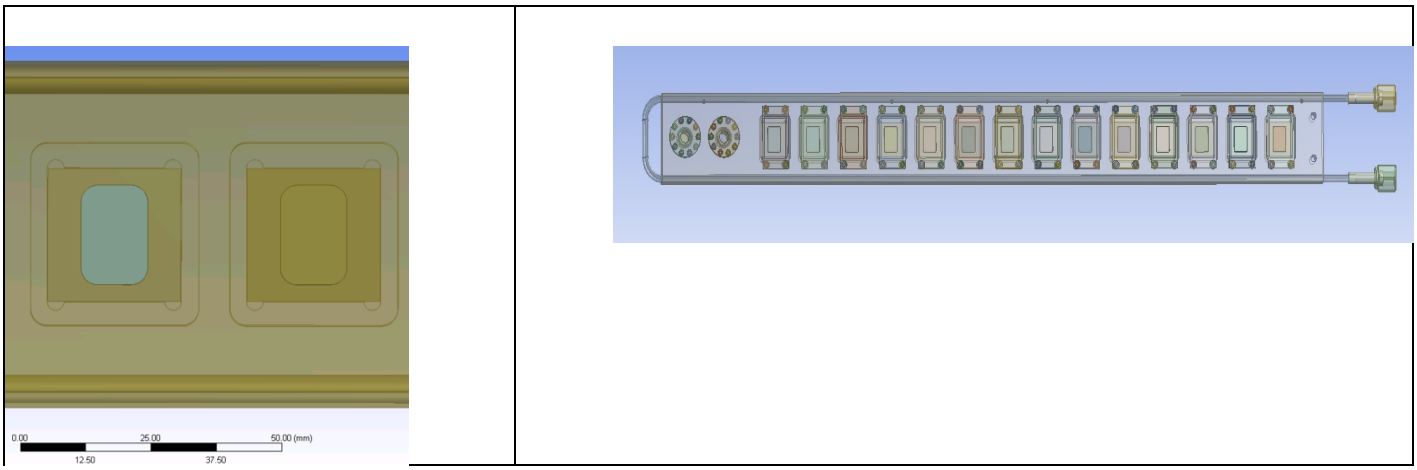

Figure 3.4: Beam view of the target showing 2 targets on the left and the whole PREX2/CREX target ladder on the right. A ^{208}Pb foil surface is 25 mm by 25 mm. The beam clear surface of a target foil is 12 mm by 19 mm (the rest is in contact with the Cu frame). The Cu frame has the coolant Cu tube brazed on its perimeter (visible in the pictures). The PREX2 motion system can move the target ladder horizontally and the range of motion can accommodate up to 16 targets (for calibrations, beam alignment, optics etc.).

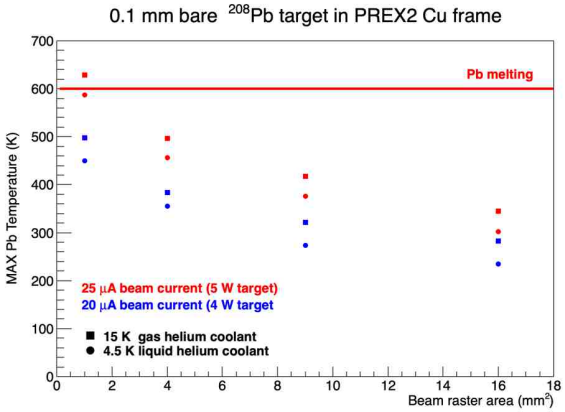

Figure 3.5: Summary of CFDFAC predictions for maximum temperature in a 0.1 mm thick bare ^{208}Pb target mounted in the PREX2 target copper frame versus beam square raster area. There are two beam currents considered: 25 μA in red and 20 μA in blue. For each beam current there are two coolant temperatures considered: 15 K helium gas in solid squares and 4.5 K liquid helium in solid circles.

In Fig. 3.5 if the beam raster area is 9 mm^2 CFDFAC predicts that the maximum temperature in the ^{208}Pb target would be 418 K at 25 μA with GHe coolant and 273 K at 20 μA with LHe coolant. The PREX2 target design could be the prototype target for the proposed experiment. The PREX2 target chamber and its motion mechanism would be available. The collaboration will study the feasibility of interfacing the PREX2 target chamber with the downstream beamline. The lessons learned from the CFD design and successful beam operation of the PREX2 target will be applied in the design of the HyperNuclear Pb target. More information on the CFDFAC target design can be found in the Target Appendix.

We will setup a system that allows to monitor continuously the target thickness when is exposed to beam. At NIKHEF the temperature was monitored by a pyrometer setup. This instrument measured a temperature of 394-414 Kduring the experiment which was conveniently below the melting temperature of lead (601 K).

For our experiment we plan to monitor the target thickness by performing elastic scattering measurement off Pb-208.

During data taking, we will monitor continuously the thickness of the target by measuring electron scattering rate as a function of two-dimensional positions by using raster information. This method was already used for the CH_2 targets in Hall-C hypernuclear programs and cracking or melting of the target were monitored to know right time for target exchange. We will monitor the temperatire of the targe also with a pyrometer (see Appandix 1 for details.

5. Particle identification

The identification of kaons detected in the hadron arm together with a huge background of protons and pions is one of the major challenge of the experiment. To reduce the background level in produced spectra, a very efficient PID system is necessary for unambiguous kaon identification. In the electron arm, the Gas Cherenkov counters [33] give pion rejection ratios up to 10^3. The dominant background (knock-on electrons) is reduced by a further 2 orders of magnitude by the lead glass shower counters, giving a total pion rejection ratio of 10^5. The lead-glass shower counters and the gas Cherenkov are calibrated against each other.The PID system in the hadron arm of HKS is composed of: three planes of time-of-flight counters, two planes of water Cerenkov counters, and three planes of aerogel Cerenkov counters. Accidental *e'K*+-coincidence events would be a background in a resulting missing-mass spectrum.

An upper limit for the accidental π^+ and proton background events is provided by the yields of the last hypernuclear experiment at JLab Hall C (E05-115). In this experiment with a 0.2-g/cm^2 ^7Li target and a beam current of 32 μA, the counting rates in the spectrometer HKS were: $K^+ : \pi^+ : p = 300 : 25000 : 34000$ Hz. The expected rates of π^+_s and protons in the spectrometer PCS + HKS during the experiment

proposed here will be smaller than these figures, because of the smaller number of nuclei present in the lead target and the smaller beam current that compensate for the bigger number of protons present in Pb nuclei. The HKS has Cherenkov counters with radiation media of aerogel (n = 1.05) and water (n = 1.33) to reject π^+_s and protons. The Cherenkov counters reduced the fractions of π^+_s and protons down to 0.5% and 10%, respectively, at the trigger level. In off-line analysis, π^+_s and protons could be reduced to 4.7×10^{-4} and 1.9×10^{-4} by using information on light yields in the Cherenkov counters and reconstructed particle-mass squared. The most important off-line analysis for K^+ identification (KID) is a time-of-flight (TOF) analysis. The TOF from the target to the timing 23 counter was 10 m in HKS, and the TOF resolution was $\sigma = 0.26$ ns. Thus, a time separation of K^+_s from π^+_s and protons at 1.2 GeV/c were more than 6σ and 20σ respectively when an event selection was applied to select the e ′K^+ coincidence with a time gate of ±1 ns. The KID performance of HKS in the present experiment without any an additional detector will be the same as achieved in E05-115 since the central momentum is the same. Therefore, accidental coincidence events in the missing mass spectrum originated mainly from e ′K^+ coincidences generated by quasi-free Λ and Σ^0 production. The K^+ rate in the present experiment R_K is estimated assuming that the production-cross section of quasi-free Λ is proportional to $A^{0.8}$:

$$R_K = R_K^{ref} \times \frac{0.1}{0.2} \times \frac{25}{32} \times \frac{\Gamma^{int}}{\Gamma_{ref}^{int}} \times \frac{208^{0.8}}{7^{0.8}} \times \frac{7}{208} \qquad (7)$$

where 32, 0.2, and 7 are the beam current, target thickness and target atomic number in the experiment E05-115 respectively, 25, 0.1, and 208 are the corresponding numbers for the experiment proposed here, $\Gamma_{ref}^{int} = 5.67 \times 10^{-5}$ and $\Gamma^{int} = 1.7 \times 10^{-5}$ are the integrated virtual photon flux in the experiment E05-115 and in the experiment proposed here respectively, and $R_K^{ref} = 300$ Hz is the K^+ rate in the experiment E05-115. Similarly, e ′ rates $R_{e'}$ in HRS were estimated from that in the E05-115 experiment: $R_{e'}^{ref} = 2.2 \times 10^6$ Hz, assuming a major contribution comes from Bremsstrahlung process. For the estimation, a rate-reduction effect due to the smaller acceptance of HRS compared to that of the e ′ spectrometer in E05-115 (HES) was also taking into account. The resulting expected singles rates of scattered electrons and K^+_s in HRS and HKS are $R_{e'} = 5200$ Hz and $R_K = 18$ Hz respectively. The accidental K^+ cross section, h_{acc}^{ref}, in the missing mass spectrum of ${}^7Li(e,e'K^+){}^7_\Lambda He$ reaction of the experiment E05-115 was about 6.5 [(nb/sr)/0.375 MeV]. For the present experiment, the accidental coincidence background cross section h_{acc} is estimated as $h_{acc} = h_{acc}^{ref} \times \frac{R_{e'}}{R_{e'}^{ref}} \times \frac{R_K}{R_K^{ref}} = 0.0025$ [(nb/sr)/MeV] and the expected accidental K^+ rate is < 0.1 events/MeV/day.

The Hall A RICH detector might be added to improve the kaon identification. We would have a pion-kaon power rejection ~ 10^{12} **(see Appendix 2 for details)**

5.1 Expected missing mass resolution

The following factors contribute to the total mass resolution of the (e,e'K^+):

1. Spectrometers' momentum and angle resolution.
2. Beam energy resolution, assumed to be $dE/E < 5 \times 10^{-5}$ for a 4.5 GeV electron beam.
3. Kinematic broadening due to uncertainty of the K^+ and e' scattering angles originated from multiple scattering through the materials between the target and tracking chambers in addition to the angular resolution of the spectrometer itself.
4. Energy loss and straggling in the target.

Since our vertex resolution is not enough to determine the reaction point in the solid target (typically the thickness is less than a half mm while the gaseous target thickness is 200 mm), so energy loss of charged particles can becorrected only as an average. Its distribution including straggling will contribute the final mass resolution. For kaons, both the energy loss distribution due to the reaction point distribution and straggling will contribute while the sum of energy losses in the target for the beam and scattered electron is roughly constant and thus only straggling is problem.

The missing mass resolution was estimated by Monte Carlo (MC) GEANT4 simulations. In these simulations scattered electrons and produced kaons were generated at the target position with momenta and scattering angles randomly chosen in the spectrometer acceptances around the kinematics values of the reaction $^{208}Pb(e,e'K^+)^{208}_{\Lambda}Tl$. Scattered electrons and produced kaons were then tracked inside the spectrometer PCS + HRS and PCS + HKS respectively up to the detectors placed at focal the planes of the spectrometers. Taking into account realistic position and angular resolutions of the particle detectors, the information of particle positions and angles at the focal planes were converted into momentum vectors at the production point by using backward transfer matrices. In these simulations magnetic field maps generated by the finite element calculation software, Opera3D (TOSCA), were used. The estimated momentum and angle resolutions of the spectrometers PCS + HKS and PCS + HRS are summarized in Table V. As a result, the missing mass resolution was conservatively estimated of the order of 0.8 MeV FWHM.

The missing mass resolution was estimated by Monte Carlo (MC) GEANT4 simulations. In these simulations scattered electrons and produced kaons were generated at the target position with momenta and scattering angles randomly chosen in the spectrometer acceptances around the kinematics values of the reaction $^{208}Pb(e,e'K^+)^{208}_{\Lambda}Tl$. Scattered electrons and produced kaons were then tracked inside the spectrometer PCS + HRS and PCS + HKS respectively up to the detectors placed at focal the planes of the spectrometers. Taking into account realistic position and angular resolutions of the particle detectors, the information of particle positions and angles at the focal planes were converted into momentum vectors at the production point by using backward transfer matrices. In these simulations magnetic field maps generated by the finite element calculation software, Opera3D (TOSCA), were used. The estimated momentum and angle resolutions of the spectrometers PCS + HKS and PCS + HRS are summarized in Table V. As a result, the missing mass resolution was conservatively estimated of the order of 0.85 MeV FWHM.

Table V Expected spectrometer resolutions and their contribution to missing mass resolution.

	Momentum/Energy Resolution (%)	Angle resolution (mrad)	Contribution to the missing mass resolution (keV)
PCS + HKS	4.2 x10^{-4}	0.6	500
PCS + HRS	2x10^{-4}	1.5	600
Beam	5x10^{-5}	-	250
Missing Mass Resolution			850

5.2 Expected yield and required beam time

The ^{208}Pb experiment, if approved would run together with the approved E12-15-008, so, for sake of completeness, we report here the beam time needed for calibration runs (solid targets thicknesses are normalized to be 100 mg/cm^2) requested for that experiment experiment. The beam time has been estimated to have enough events for major shell peak energies to be statistically determined with an accuracy of 50 keV. We are adding up here the bem time needed for the calibration run for the ^{208}Pb target
We are asking for 20 days for ^{208}Pb experiment. The Signal to Noise Ratio (SNR) is very high even for the s shell peak

Yields estimation and beam time requirement.

Target and objective hypernucleus	Beam current (μA)	Target thickness (mg/cm^2)	Assumed cross section (nb/sr)	Expected Yield (/hour)	Num. of events	Req. beamtime (hours)	B.G. Rate (/MeV/h)	S/N (±4 σ)	Comments
CH_2	2	500	200	19	1000	54	0.05	252	Calibration
^{6,7}Li	50	100	10	5.4	150	28	1.3	4.9	Calibration
^{9}Be	100	100	10	36	300	9	4.7	8.8	Calibration
^{10,11}B	25	100	10	16	150	19	0.29	33	Calibration
^{12}C	100	100	100	54	2000	37	4.4	17	Calibration
Subtotal for calibration						147			
^{208}Pb	**25**	**100**	**80(g.s.)**	**0.3**	**145**	**480**	**0.1**	**15**	**Production**

The counting rate and consequentely the beam time requested evaluation is based on the x-sections re-evaluated by T. Motoba for the new kinematics. The x-sections are much higher than the ones of the previous kinematics (by a factor of 8-10).

5. Summary and conclusion

Based on more than a decade of experience at JLab, Hall A and Hall C, the JLab Hypernuclear Collaboration proposes the $^{208}Pb(e,e'K^+)^{208}_{\Lambda}Tl$ experiment complementary to the $^{40}Ca(e,e'K^+)^{40}_{\Lambda}K$ and $^{40}Ca(e,e'K^+)^{40}_{\Lambda}K$ for studying the hyperon puzzle.

We showed that for astrophysical implications, particularly for the neutron star puzzle critical additional information can be obtained by expanding the kaon electroproduction program to include a study of the ^{208}Pb(e,e'K$^+$)$^{208}_{\Lambda}$Tl reaction. In fact thanks to the extended region of constant density and the large neutron excess, ^{208}Pb provides the best available proxy of neutron star matter. The solution of neutron star puzzle requires a better understanding of the YN interaction in a wide range of systems, from light to medium and heavy hypernuclei, as well as the development of a consistent framework allowing for accurate theoretical calculation. To "solve" the hyperon puzzle you need strong repulsive forces

The use of a ^{208}Pb target will allow to investigate hypernuclear dynamics in a new environment, in which three-body interactions are expected to play an important role. We underline that in the non strange sector the contribution of three-nucleon forces (needed to address the "hyperon puzzle"), which is known to be large and repulsive in nuclear matter at equilibrium density, is believed to be much smaller and attractive in ^{40}Ca [Lonardoni2017

In addition, the availability of accurate ^{208}Pb(e, e'p)^{207}Tl data will allow to exract the Λ binding energies from the measured (e,e'K$^+$) cross section using a largely model independent procedure. The results of this analysis will provide essential information, needed to constrain and improve the available models of the YN and YNN potentials.

We have shown that the experiment will achieve very high Signal to Noise (SNR) for all the peaks to be detected, as well as very good missing mass resolution (~ 800 kev) and precision (~ 70 keV) in identifying the postion of the peaks

The experiment will utilize well-established magnetic spectrometers HRS and HKS that were successfully used in the previous hypernuclear programs in Hall A and Hall C (*see Apendix 3*)

Appendix 1

Target Appendix

The Computational Fluid Dynamics FACility (CFDFAC) has designed two prototype targets for the PREX2 experiment, a static one (as shown in Fig. 3.1) and a rotating one (as shown in Fig. A.3). In both designs the target is cryogenically cooled. The design beam parameters were: current up to 100 μA, minimum beam raster area on target 16 mm^2, minimum intrinsic beam diameter 160 μm. The static target is a sandwich diamond-Pb-diamond (C-Pb-C), while the rotating target can be bare Pb. CFDFAC has performed both steady-state and time-dependent thermal simulations of beam heating for both prototypes to map out the available phase space for safe operations in beam current, intrinsic beam diameter, beam raster area, beam raster control frequencies, cooling capacity and target internal contacts quality (Pb-diamond and diamond-copper frame or Pb-copper frame). While it would have been desirable to have a bare Pb target in beam, for PREX2 having diamond foils in beam along with Pb amounted to an extra background whose dilution factor and parity violation asymmetry could be measured with desired precision and corrected for. The PREX2 collaboration decided to run with the static target design, which worked as predicted.

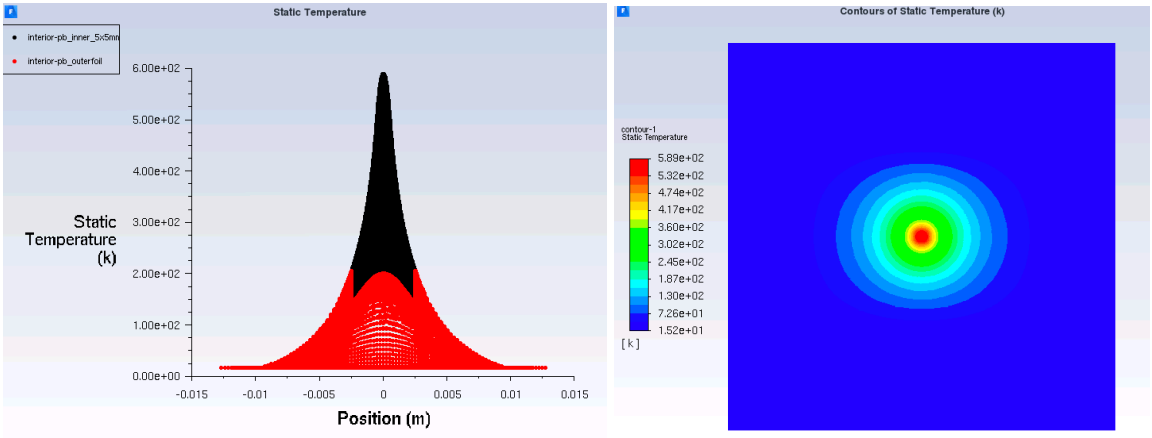

Figure A.1: Temperature profile in a prototype bare ^{208}Pb target 0.1 mm thick with a surface 25 mm by 25 mm hit by a 25 μA beam current rastered over a square area on the target with side 1 mm. The Pb foils is installed in the PREX2 target Cu frame and cooled with 4.5 K LHe. The plot on the left is a 1D projection of the 2D temperature profile on the right. For the left plot the Pb target is divided into two regions: a square of side 5 mm at its center (black) and the rest of the target (red).

The predicted temperature profile in the ^{208}Pb target at 25 μA beam rastered over a square area of side 1 mm at the target, cooled by a flow of 4.5 K LHe is shown in Fig. A.1. This represents the one data point in the Fig. 3.2: the solid red circle at raster area 1 mm^2. CFDFAC predicts that a 25 μA beam current rastered over such a small area would most probably melt the target, even with LHe cooling.

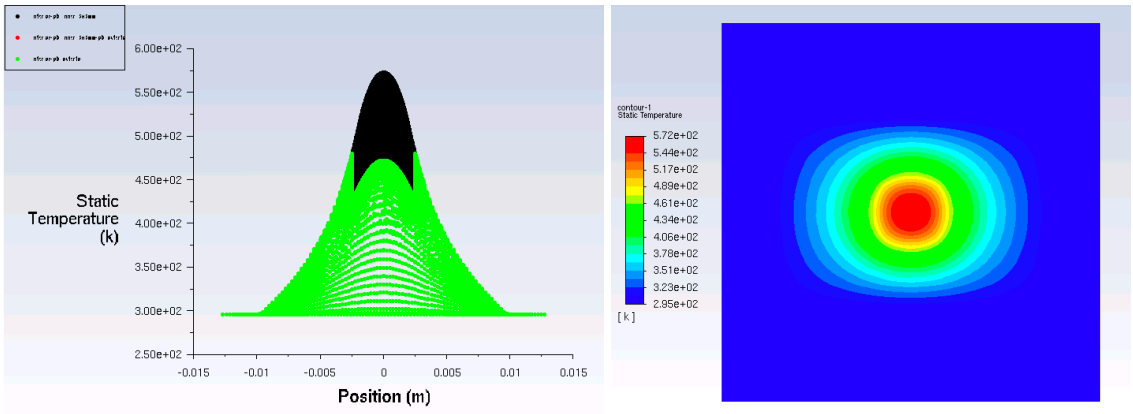

Figure A.2: Temperature profile in a prototype bare ^{208}Pb target 0.1 mm thick with a surface 25 mm by 25 mm hit by a 20 μA beam current rastered over a square area on the target with side 4 mm. The Pb foils is installed in the PREX2 target Cu frame and cooled with 295 K water. The plot on the left is a 1D projection of the 2D temperature profile on the right. For the left plot the Pb target is divided into two regions: a square of side 5 mm at its center (black) and the rest of the target (red).

The predicted temperature profile in the ^{208}Pb target at 20 μA beam rastered over a square area of side 4 mm at the target, cooled by a flow of 295 K water is shown in Fig. A.2. This is comparable with the predictions and measurements made by C. Marchand et al. [MARCHAND] for their water cooled target at NIKHEF. CFDFAC predicts that a 20 μA beam current rastered over a 16 mm^2 area and with water cooling would probably melt the target.

CFDFAC has done extensive CFD simulations to prototype a high beam current rotating Pb target for PREX2. One such model is shown in Figure A.3-left, where the Pb target is mounted on a cylindrical Cu holder, which can rotate about its axis and it is cooled to 15 K. Figure A.3-right shows the CFD temperature profile calculation through the Pb and Cu from heating with a 70 μA electron beam rastered on a square of side 2 mm on the Pb target rotating at 0.5 Hz. The Cu holder is assumed sinked to 15 K.

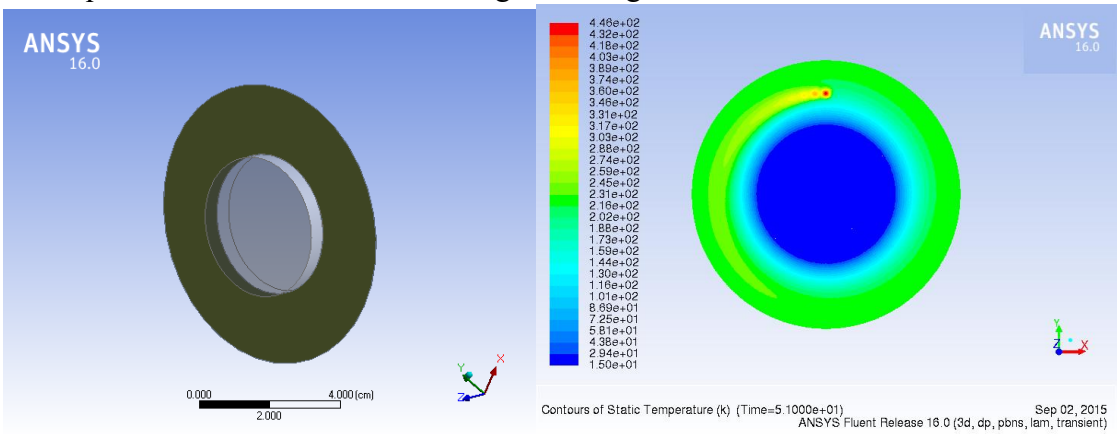

Figure A.3: Rotating target model. Left: The Pb wafer is the outer annulus, while the inner 4 cm diameter cylinder is the wafer holder made of Cu. Right: Temperature profile in cross section through the Pb target and its Cu holder rotating at 0.5 Hz produced by a 70 μA electron beam rastered on a square of side 2 mm on the Pb target.

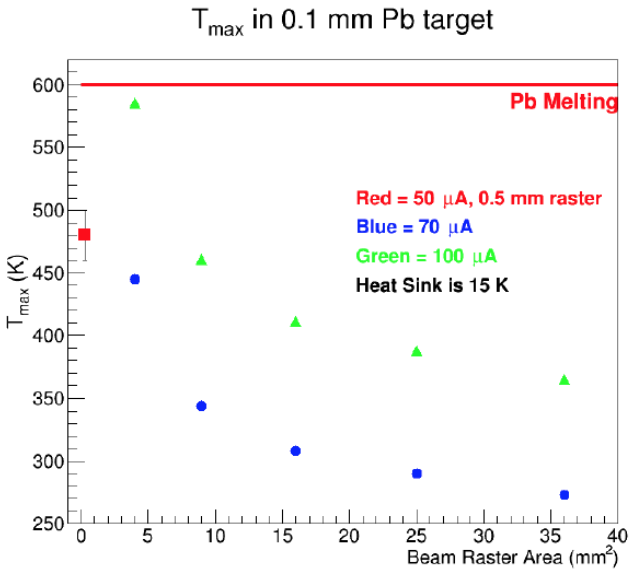

Figure A.4: Summary plot of maximum temperature in the Pb target from Figure A.3 vs. electron beam raster area at two beam currents. The red point is for unrastered electron beam of intrinsic diameter 0.5 mm at 50 μA beam current. The target rotates at 0.5 Hz. Pb melts at about 601 K as indicated by the red horizontal line in the plot.

Figure A.4 is a summary plot of the maximum temperature in the Pb rotating target in Figure A.3-right vs. beam raster area for two different beam currents and one single data point for unrastered electron beam. Figure A.4 shows that rotation and cooling prevent this model of the target from melting even at 70 μA beam current with a square beam raster of side 2 mm.

Scaling from Fig. A.4, the maximum temperature difference at 70 μA beam current at a beam raster area of 2 x 2 mm^2 to a beam current of 25 μA we estimate a maximum temperature in the Pb target at 25 μA beam current for the target rotating at 0.5 Hz of 170 K. CFDFAC has developed a prototype rotating target which has been operated with a graphite foil in air.

The CFDFAC operates a test stand that can thermally assess solid targets with high power laser heating. The test stand is currently installed in Lab 6 in FEL and consists of a vacuum chamber with a turbomolecular pump, linear motion mechanism to move targets inside the vacuum space, viewports for the laser light, vacuum ports with feedthoughs for instrumentation, high power laser with optics and data acquisition. Lasers with powers up to 30 W are currently available. The stand is instrumented with three remote temperature reading/monitoring pyrometers spanning a temperature range from 150°C to 2000°C. Direct contact temperature sensors can be instrumented as needed. This stand has been used to make a thorough thermal assessment of the tungsten foils that will be used as a primary target in the APEX experiment in Hall A at JLab. CFDFAC also operates a high performance computing (HPC) farm with 256 CPUs at JLab that is being routinely used to perform thermal studies/simulations with ANSYS CFD software engines. The CFDFAC HPC farm has been instrumental in designing the new standard liquid hydrogen targets in Halls A and C and in assessing the 3He polarized target, the tritium and argon targets, the APEX target and the PREX2/CREX targets. The stand can test static targets in vacuum and air, rotating targets in air and in future could test rotating targets under vacuum. The test stand could be used to develop a Pb target for this experiment. The stand is shown in Figure A.5.

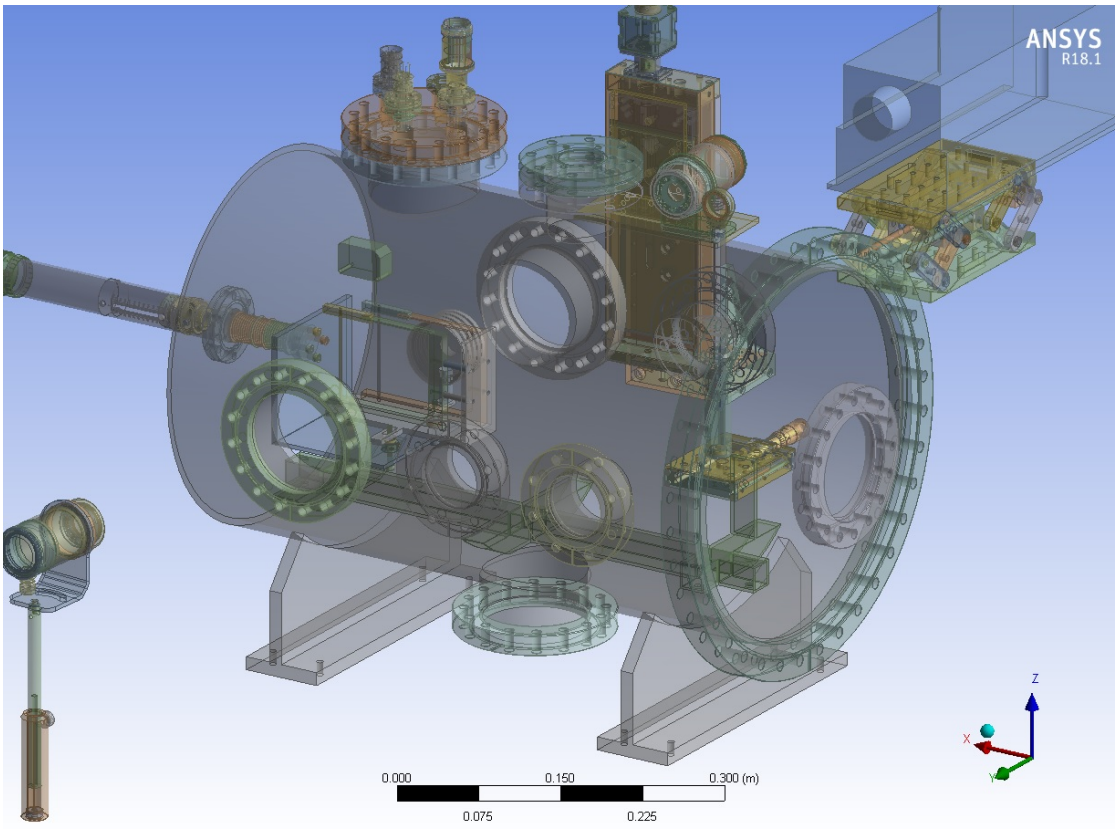

Figure A.5: CAD model of test stand to thermally assess solid targets under vacuum at JLab.

Appendix 2

PID. The RICH option

The Hall A RICH detector will be added to improve the kaon identification. The detector [27,28,29] was used successfully during the E-94-107 experiment providing a very good pion/kaon rejection at 2 GeV/c better than 1:1000 (corresponding to a pion/kaon angle separation of ~ 6.0 sigma) [27,28,29].

The layout of the RICH is conceptually identical to the ALICE HMPID design [34]. It uses a proximity focusing geometry, a CsI photocathode, and a 15 mm thick liquid Freon radiator. A detailed description of the layout and the performance of the detector is given in [23, 24, 25]. After the E-94-107 experiment the detector was upgraded to match the needs of the Transversity approved experiment (E06-011) to be able to identify kaons of 2.4 GeV/c. [30]. The upgrade extended the performance by means of a larger photon detector (a multiwire-multipad proportional chamber) and a longer proximity gap which improved the photon detection geometrical efficiency and the angular resolution, respectively.

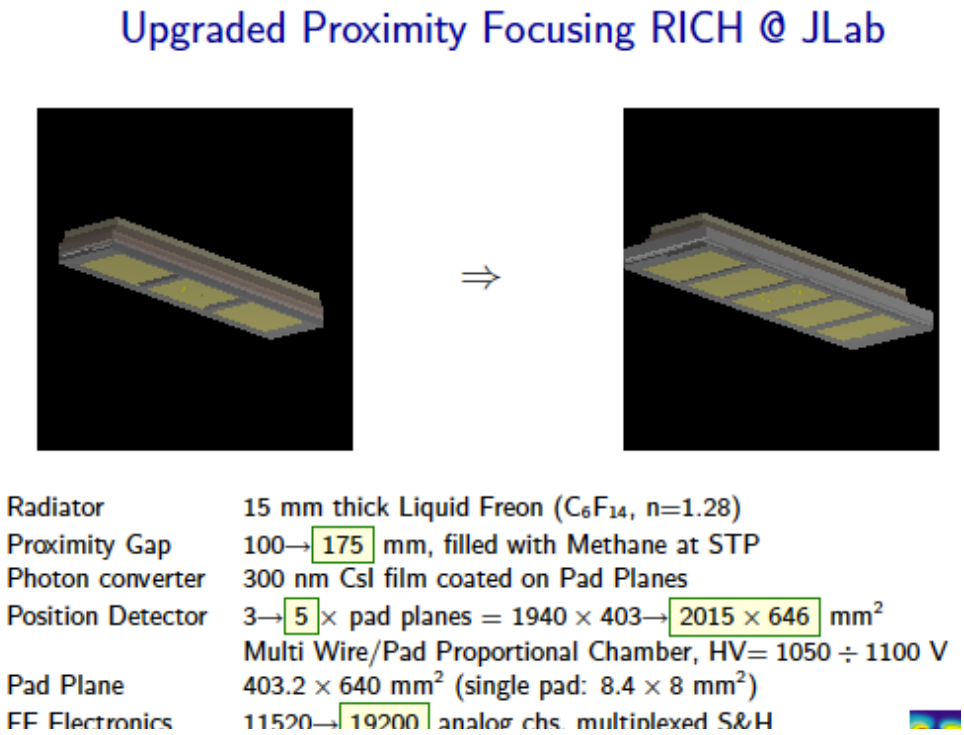

Fig. A1. Old and new upgrated RICH layout

In Fig. A1 we show the old and new (upgrated) layout. The photon detection plane was doubled (3 more pad panels added). This would have allowed the detectors to separate kaons, in the E-94-107 kinematical conditions (at a kaon momentum ~ 2 GeV/c) with a higher rejection ratio, an additional ~ 1.5 sigma (Fig.10,11) corresponding to a pion:kaon rejection better than 1:10000 at 2.0 GeV/c, with improved efficiency.

In our experiment the central momentum of the detected kaons will be 1.2 GeV/c. For this reason even better performances to separate kaons from pions will be obtained. Easy calculation **[37]** bring to ~ 7.8 sigma the pion – kaon separation angle. Adding conservatively 1.5 sigma, we would obtain a separation ~ 9.3 sigma. This would correspond, assuming a factor ~ 100 for pion-kaon particle population, to a ~ 10^6 power rejection

Convoluting the threshold Cherenkov and the RICH power rejection we would have a pion-kaon power rejection ~ 10^{12}

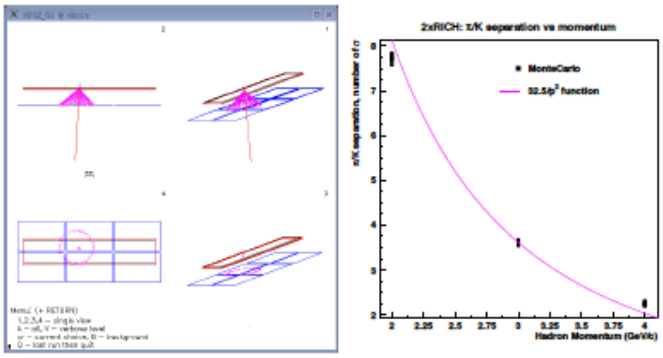

Fig. A2 Upgraded RICH simulation events (left panel) and expected performance (right panel): pion-kaon separation (number of sigmas) at fferent hadron momenta. The simulation is tuned to the E-94-107 hypernuclear experimental data.

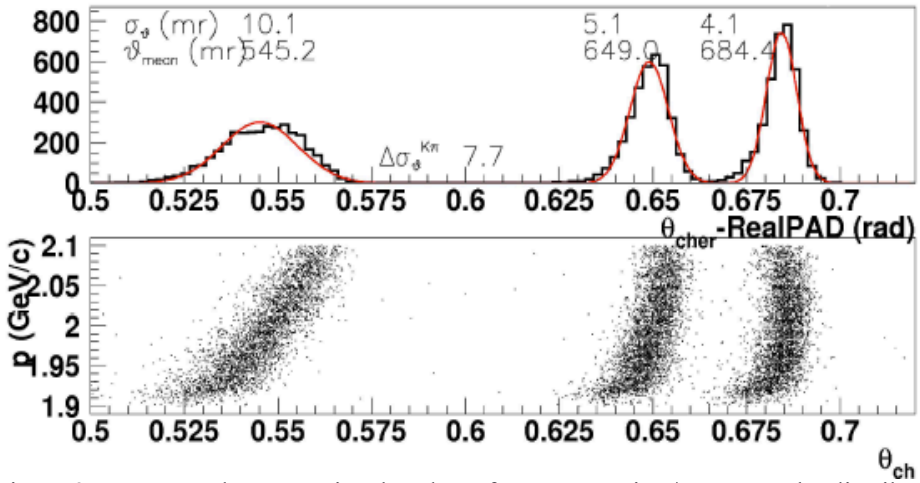

Fig. A3. Upgrated RICH simulated performance. Pion/Kaon angle distribution (equal hadrons populations) at 2 GeV/c momentum, in the HRS acceptance. The Mcarlo is tuned on Hall A hypernuclear experimental data.

Appendix 3

The experiment will utilize well-established magnetic spectrometers HRS and HKS that were successfully used in the previous hypernuclear programs in Hall A and Hall C. Here we report the main parameters for conducting the experiment

Key Experimental Parameters:

Beam energy: 12 GeV mode, 2-pass: 4.5238 GeV, Hall-A,

Requested beam time in total: 480 hours (20 days)

Beam current: 25 μA,

Major apparatus: HKS, HRS, and PCS

Required resources: Major installations and new support structures:

HKS and PCS need major installation of magnets and detector packages,

HKS needs a new support for Hall A.

(New support structure for the Septa and Shielding houses for detectors are necessary.)

Major Equipment:

Magnets: HRS in Hall A, HKS (KQ1, KQ2 and KD), new Septum magnets

Power Supplies: HKS-D (252V, 1254A), HES-D (250V, 1100A) have own PS's provided by Tohoku University, all other PS's necessary are to be prepared by JLab.

Targets: Solid targets (CH_2, ^{6,7}Li, ^{9}Be, ^{10,11}B, ^{12}C, ^{40}Ca, ^{48}Ca, ^{208}Pb). **The ^{208}Pb target has to have cryogenic cooling in a standard way (as PREX target)**

Detectors: Standard detectors for HRS and HKS-detector package (Drift Chambers, TOF walls, Aerogel Cherenkov, Water Cherenkov.)

Electronics: Standard electronics, F1-TDCs, Amp-discriminator cards for drift chambers, FPGA based special trigger modules developed by Tohoku University (TUL-8040).

Computer Hardware: Standard

Possible Hazard

Electrical Equip.: high voltages for PMT, Drift Chambers, large currents for magnets

Flammable gas for drift chambers: Argon Ethane 50/50, 0.15 l/min each for HRS and HKS.

Targets: Condition 1, 2 are for single spectrometer calibration with elastic scattering. Condition 3-7 are for calibration with coincidence measurement, 8-12 are for the physics run with gaseous cryogenic target

Condition #	Beam Energy (MeV)	Beam Current (μA)	Special Request	Target Material	Material Thickness (mg/cm^2)	Est. Beam on time (hours)
1	1200	10		Ta	100	10
2	3000	10		Ta	100	10
Single Arm. Calib						**20**
3	4523.8	2	2 × 2 mm^2 raster	CH_2	500	54
4	4523.8	50	2 × 2 mm^2 raster	^{6,7}Li	100	28
5	4523.8	100	No raster	^{9}Be	100	9
6	4523.8	25	2 × 2 mm^2 raster	^{10,11}B	100	19
7	4523.8	100	No raster	^{12}C	100	37
Subtotal calibration						147
Pb	**4523.8**	**25**	**3x3mm^2 raster**	**^{208}Pb**	**100**	**480**

References

[MAE89] P. M. M. Maesen et al, Phys. Rev. C 40, 2226 (1989).
[RIJ99] T. A. Rijken et al., Phys. Rev. C 59, 21 (1999).
[STO99] V. G. J. Stoks et al., Phys. Rev. C 59, 3009 (1999).
[RIJ06] T. A. Rijken et al., Phys. Rev. C 73, 044007 (2006).
[RIJ06b] T. A. Rijken et al., Phys. Rev. C 73, 044008 (2006).
[HOL89] B. Holzenkamp et al., Nucl. Phys. A 500, 485 (1989).
[HAI05] J. Haidenbauer and U.-G. Meissner, Phys. Rev. C 72, 044005 (2005).
[POL06] H. Polinder, J. Haidenbaer and U.-G. Meissner, Nucl. Phys. A 779, 244 (2006).
[HAI20] J. Haidenbauer, U.-G. Meissner and A. Nogga, Eur. Phys. Jour. A 56, 91 (2020).
[HAI20b] J. Haidenbauer and I. Vidaña, Eur. Phys. Jour. A 56, 55 (2020).
[LOG19] D. Logoteta, I. Vidaña and I. Bombaci, Eur. Phys. J. A 55, 207 (2019).
[Benhar2016] O. Benhar, Nucl. Phys. News **26**, 15 (2016)
[Benhar2020] O. Benhar, "Extracting Hypernuclear Properties from the (e,e'K^+) Cross Section" (paper in praparation, see http://www.jlab.org/indico/event/386/timetable/)
[Bydžovský2018] D. Skoupil and P. Bydžovský Phys. Rev. C **97**, 025202 (1918)
[Bydzovsky2012] P. Bydžovský et al Electromagnetic production of medium-mass Λ, Nuclear Physics A 881 (2012) 199–217
[Vidaña2017] I. Vidaña, Nucl. Phys**.** A **958**, 468 (2017)
[LONA2017]D. Lonardoni *et al*, Phys. Rev. C **96**, 024326 (2017)
[BOM16] I.Bombaci, ArXiv:1601.05339; HYP2015 Proceedings.
[AMB60] V. A. Ambartsumyan and G. S. Saakyan, Sov. Astron. AJ 4, 187 (1960).
[THO99] S. E. Thorsett and D. Chakrabarty, Astrophys. J. 512, 288 (1999).
[DEM10] P. B. Demorest, *et al.*, Nature 467, 1081 (2010).
[ANT13] J. Antoniadis, *et al.*, Science 340, 1233232 (2013).
[VID11] I. Vidana, D. Logoteta, C. Providencia, A. Polls, and I. Bombaci, Europhys. Lett. 94, 11002 (2011).
[HJS11]H.-J. Schulze and T. Rijken, Phys. Rev. C 84, 035801 (2011).
[MAS12] E. Massot, J. Margueron, and G. Chanfray, Europhys. Lett. 97, 39002 (2012).
[BED12] I. Bednarek, *et al.*, Astron. Astrophys. 543, A157 (2012).
[WEI12] S. Weissenborn, D. Chatterjee, and J. Schaffner-Bielich, Phys. Rev. C 85, 065802 (2012);
[MIY13] T. Miyatsu, M.-Ki Cheoun, and K. Saito, Phys. Rev. C 88, 015802 (2013);
[LOP14] L. L. Lopes, and D. P. Menezes, Phys. Rev. C 89, 025805 (2014).
[WIR95] R. B. Wiringa, V. G. J. Stoks, and R. Schiavilla, Phys. Rev. C 51, 38 (1995);
R. B. Wiringa and S. C. Pieper, Phys. Rev. Lett. 89, 18 (2002).
[MAC96] R. Machleidt, F. Sammarruca, and Y. Song, Phys. Rev. C 53, R1483 (1996).
[EPE05] E. Epelbaum, W. Glockle, and Ulf-G. Meissner, Nucl. Phys. A 747, 0375 (2005).
[EKS13] A. Ekstrom et al., Phys. Rev. Lett. 110, 192502 (2013).
[GEZ13] A. Gezerlis et al., Phys. Rev. Lett. 111, 032501 (2013).
[MIW11] K. Miwa *et al.,* J-PARC E40 experiment.
[PIE08] S. C. Pieper, AIP Conf. Proc. 1011, 143 (2008); Nuovo Cimento Rivista Serie 31, 709 (2008).
[MAR13] P. Maris, J. P. Vary, S. Gandolfi, J. Carlson, and S. C. Pieper, Phys. Rev. C 87, 054318 (2013).
[PUD95] B. S. Pudliner, V. R. Pandharipande, J, Carlson, R. B. Wiringa, Phys. Rev. Lett. 74, 4396 (1995).
[GAN12] S. Gandolfi, J. Carlson, and S. Reddy, Phys. Rev. C 85, 032801 (2012);
S. Gandolfi, J. Carlson, S. Reddy, A. W. Steiner, and R. B. Wiringa, Eur. Phys. J. A 50, 10 (2014).
[NAG14] MM.Nagels, Th.A.Rijen, Y.Yamamoto, arXiv:1408.4825.
[FUR09] T. Furumoto, Y. Sakuragi, Y. Yamamoto, Phys. Rev. C 79 (2009) 0011601(R).

[LON14] D. Lonardoni, F. Pederiva, and S. Gandolfi, Phys. Rev. C 89, 014314 (2014).
[NAG15] MM.Nagels, Th.A.Rijen, Y.Yamamoto, arXiv:1501.06636.
[HAI13] J.Haidenbauer et al., Nucl. Phys. A 915 (2013) 24.
[PED15] F. Pederiva, F. Catalano, D. Lonardoni, A. Lovato and S. Gandolfi, arXiv:1506.04042.
[BOD84] A. R. Bodmer, Q. N. Usmani, and J. Carlson, Phys. Rev. C 29, 684 (1984);
A. R. Bodmer and Q. N. Usmani, Phys. Rev. C 31, 1400 (1985); A. R. Bodmer and
Q. N. Usmani, Nucl. Phys. A 477, 621 (1988).
[USM95] A. A. Usmani, S. C. Pieper, and Q. N. Usmani, Phys. Rev. C 51, 2347 (1995); A. A. Usmani,
Phys.Rev. C 52, 1773 (1995); Q. N. Usmani and A. R. Bodmer, Phys. Rev. C 60, 055215 (1999);
A. A. Usmani and F. C. Khanna, J. Phys. G 35, 025105 (2008).
[IMR14] M. Imran, A. A. Usmani, M. Ikram, Z. Hasan, and F. C. Khanna, J. Phys. G 41, 065101 (2014).
[LON15] D. Lonardoni, A. Lovato, S. Gandolfi, and F. Pederiva, Phys. Rev. Lett. 114, 092301 (2015).
[YAM14] Y. Yamamoto, T. Furumoto, N. Yasutake and Th.A. Rijken, Phys. Rev. C 90 (2014) 045805.
[ISA16] M.Isaka, Y.Yamamoto and Th.A.Rijken, presentation at JLab Hypernuclear workshop (2016).
[PIL91] P. Pile *et al.* , Phys. Rev. Lett. **66** (1991) 2585.
[HOT01] H. Hotchi, *et al.* Phys. Rev. C 64, 044302 (2001).
[GOG16] T.Gogami et al., Phys. Rev. C 93, 034314 (2016).

[EUR16] EurekAlert! "New spectroscopy of $^{10}\Lambda$Be hypernucleus redfines the reference data
of Lambda hypernuclei", http://www.eurekalert.org/pub_releases/2016-04/tu-nso040616.php
[Fro]B. Frois and C. N. Papanicolas, Ann. Rev. Nucl. Part. Sci. **37**, 133 (1987)
[Quint]Quint et al, E. N. Quint et al., Phys. Rev. Lett. **58**,
1727 (1987).
[Baten]M. van Batenburg, PhD Thesis, University of Utrecht, 1996.
[BEN90] O. Benhar, A. Fabrocini, and S. Fantoni, Phys. Rev. C **41**, R24 (1990).
[HASHI] "Spectroscopy of Λ hypernuclei," Review paper, O. Hashimoto and H. Tamura,
Progress in Particle and Nuclear Physics 57 (2006).
[Hasega]T. Hasegawa et al, Phys. rev C53 (1996) 1210
[SLA] J.C. David, C. Fayard, G.-H. Lamot, B. Saghai, **Phys. Rev. C 53**, 2613 (1996);
[Quint] E. Quint, Ph.D. "Limitationd of the Mean – Field Description for nuclei in the
Pb-region, obeserved with the (e,e'p) Reaction". Thesis Universiteit van Amsterdam 1988.
[Bobel] I. Bobeldij et al. "High-Momentum Protons in 208Pb" Phys. Rev. 73, NUMBER 20 (1994)
pg. 2684-2687
[BENA1] Extracting Hypernuclear Properties from the (e, e'K^+) Cross Section *(in preparation)*
[NAKA]O. Hashimoto, S.N. Nakamura, L. Tang and J. Reinhold, JLab proposal for E01-011
[HASHI2010] O.Hashimoto et al., Nuclear Physics A835 (2010) 121.
[TANG115] O. Hashimoto, S.N. Nakamura, L. Tang and J. Reinhold, JLab proposal for E05-115
[SHARMA] B. Sharma, Q.N. Usmani and A.R. Bodmer, arXiv:110 2.1542
[Dover]C.B. Dover, Proc. Int. Sympo. on Medium Energy Physics, Beijing. World Scientifics, Singapore,
1987, p. 257
[YAMA] Y.Yamamoto, H.Bando, J.Zofka, Progr. Theoret. Phys 80 (1988)757)
[YAMA1] D.E. Lansky, Y.Yamamoto, Phys. Rev. C55 (1997) 2330
[Bogdan] Bogdan Wojtsekhowski, personal communication
[GARI]F. Garibaldi, S. Frullani, P. Markowitz and J. LeRose, spokespersons, JLab proposal
for E94-107.
[CUSA2009]F. Cusanno et al, Phys. Rev. let. 103, 202501 (2009).
[AlCORN]J. Alcorn et al. Nucl. Instr. and Methods A 522, 294 (2004)
[IODICE] Iodice et al., Nucl. Instr. ans Methods A 553, 231 (2005)
[GARI2003]F.Garibaldi et al., Nucl. Instr. and Methods A 502, 117 (2003)
[CUSA2003]F. Cusanno et al., Nucl. Instr. And Methods A 502, 251 (2003)
[GOGA2016]T.Gogami et al., PRC 2016, DOI 10.1103/PhysRevC.93.034314)
[NAKA2015], T.Gogami, L.Tang et al., Proceeding of the 12th International Conference

on Hypernuclear and Strange Particle Physics (HYP2015), JPS Conference Proceedings, in press.
[BOB]R. Michaels, personal communication
[Marchand]C. Marchand et al, "Two-foils water cooled lead target with pyrometer temperatire reading, unpublished report
[Vidaña2017] I. Vidana, Nucl. Phys**. 958**, 468 (2017).
[GOGA2016] T.Gogami et al., PRC 2016, DOI 10.1103/Phys Rev C93 (2016) 034314
[IODICE] Iodice et al., Nucl. Instr. ans Methods A 553, 231 (2005)
[GARI2003] F.Garibaldi et al., Nucl. Instr. and Methods A 502, 117 (2003)
[CUSA2003] F. Cusanno et al., Nucl. Instr. And Methods A 502, 251 (2003)
[GARI] F. Garibaldi, S. Frullani, P. Markowitz and J. LeRose, spokespersons, JLab proposal for E94-107.
[CUSA2009] F. Cusanno et al, Phys. Rev. let. 103, 202501 (2009).
[AlCORN] J. Alcorn et al. Nucl. Instr. and Methods A 522, 294 (2004)
[NAKA2015], T.Gogami, L.Tang et al., Proceeding of the 12th International Conference on Hypernuclear and Strange Particle Physics (HYP2015), JPS Conference Proceedings, in press.
[Vidaña2017] I. Vidana, Nucl. Phys**. 958**, 468 (2017).
[Sagai96] J.C. David, C. Fayard, G.-H. Lamot, B. Saghai, **Phys. Rev. C 53**, 2613 (1996);
[Mizutani] T. Mizutani, C. Fayard, G.-H. Lamot, B. Saghai, **Phys. Rev. C 58**, 75 (1998).
[GOGA2013] T. Gogami et al. N.I.M A729 (2013)816–824
[GOGATHESYS] T. Gogami, *Doctoral Thesis*, Ä*Spectroscopic research of hypernuclei up to medium-heavy mass region*
[GOGA2016] T. Gogami *et al.* (HKS (JLab E05-115) Collaboration), *Phys. Rev. C* **94**, 021302(R) (2016).
[GOGA2018] T. Gogami *et al.*, *Nucl. Instrum. Methods Phys. Res. Sect. A* **900**, 69-83 (2018).
[TSAI] Y. Tsai, *Rev. Mod. Phys.* **46**, 4 (1974).
[LONA2017] D. Lonardoni *et al*, Phys. Rev. C **96**, 024326 (2017)